
# THE IMPACT OF WAVE-MODIFIED WIND STRESS IN AN OCEAN CIRCULATION MODEL - APPLICATION TO THE SOUTH ATLANTIC

Nicolas Germain

Dissertação de Mestrado apresentada ao Programa de Pós-graduação em Engenharia Oceânica, COPPE, da Universidade Federal do Rio de Janeiro, como parte dos requisitos necessários à obtenção do título de Mestre em Engenharia Oceânica.

Orientador: Afonso de Moraes Paiva

Rio de Janeiro
Janeiro de 2017

THE IMPACT OF WAVE-MODIFIED WIND STRESS IN AN OCEAN CIRCULATION MODEL - APPLICATION TO THE SOUTH ATLANTIC

Nicolas Germain

DISSERTAÇÃO SUBMETIDA AO CORPO DOCENTE DO INSTITUTO ALBERTO LUIZ COIMBRA DE PÓS-GRADUAÇÃO E PESQUISA DE ENGENHARIA (COPPE) DA UNIVERSIDADE FEDERAL DO RIO DE JANEIRO COMO PARTE DOS REQUISITOS NECESSÁRIOS PARA A OBTENÇÃO DO GRAU DE MESTRE EM CIÊNCIAS EM ENGENHARIA OCEÂNICA.

Examinada por:

Prof. Afonso de Moraes Paiva, Ph.D.

Prof. Carlos Eduardo Parente Ribeiro, D.Sc.

Prof. Mauro Cirano, Ph.D.

RIO DE JANEIRO, RJ – BRASIL
JANEIRO DE 2017

Germain, Nicolas

The impact of wave-modified wind stress in an ocean circulation model - Application to the south Atlantic/Nicolas Germain. – Rio de Janeiro: UFRJ/COPPE, 2017.

XI, 71 p.: il.; 29, 7cm.

Orientador: Afonso de Moraes Paiva

Dissertação (mestrado) – UFRJ/COPPE/Programa de Engenharia Oceânica, 2017.

Referências Bibliográficas: p. 41 – 44.

1. Ocean circulation models. 2. Surface waves. 3. Ocean-waves coupling. 4. Drag coefficient. 5. Momentum flux. 6. Wind stress. I. Paiva, Afonso de Moraes . II. Universidade Federal do Rio de Janeiro, COPPE, Programa de Engenharia Oceânica. III. Título.

# Acknowledgements

I would like to thank the following people: Afonso Paiva, my advisor, for the time spent and the flexibility allowed to a part time student I have been. The team of the Physical Oceanography Lab - LOF/GRUPO, with special thanks to the senior staff members Mariela, Vladimir, Guilherme and Felipe, who helped and spent time answering my questions. The secretaries Cristina and Marise. Jean Bidlot from the ECMWF for answering my numerous questions about the models used at the ECMWF. Alexander Babanin, from the Swinburne University of Technology and Nelson Violante de Carvalho from the UFRJ, who provided the initial idea for this research. My wife Rosalie, who supported me during the long indoor week-ends dedicated to study and research. My company Bureau Veritas and especially Rogério Cabral, Julio Veneroso and my direct colleagues who allowed me some precious time off. And finally Brazil, for the warm welcome and the possibility given to me to continue going to the University while working.

Resumo da Dissertação apresentada à COPPE/UFRJ como parte dos requisitos necessários para a obtenção do grau de Mestre em Ciências (M.Sc.)

# O IMPACTO DA TENSÃO DO VENTO MODIFICADA POR ONDAS EM UM MODELO DE CIRCULAÇÃO OCEÂNICA - APLICAÇÃO AO ATLANTICO SUL

Nicolas Germain

Janeiro/2017

Orientador: Afonso de Moraes Paiva

Programa: Engenharia Oceânica

Uma parametrização da tensão do vento dependente das ondas de superfície foi introduzida no modelo de circulação oceânico HYCOM. O processo físico que rege essa parametrização é o crescimento e a dissipação do campo de ondas. Dois experimentos numéricos foram realizados para a região do Oceano Atlântico Sul: um com o novo efeito devido às ondas e um de controle, sem informação das ondas e utilizado como referência para comparação. Todos os campos de forçantes foram produzidos com base nos dados da reanálise ERA-20C do ECMWF. Uma caracterização espacial e temporal do fluxo de quantidade de movimento sob influência das ondas mostrou, em média, um fluxo mais fraco para todo o domínio (-7% de diferença de tensão). Eventos positivos, nos quais a tensão modificada pelas ondas é mais intensa que a tensão clássica, acontecem durante intensas tempestades, principalmente na região sul do domínio (até +59% de diferença de tensão). A resposta oceânica de longo prazo à diferença de tensões mostra uma forte modificação da TSM em duas áreas específicas: a Confluência Brazil Malvinas (até -0.9 graus) e a Ressurgência de Benguela (até +1.1 graus). As diferenças de TSM são consistentes com os processos físicos sendo modificados pelas ondas (por exemplo, nos casos citados a modificação no bombeamento de Ekman). Os processos físicos relativos às ondas responsáveis por eventos positivos são ilustrados durante duas tempestades: uma na parte sul do domínio e uma perto da costa brasileira. Diferenças positivas intensas da corrente em superfície são registradas, com valores de até 0,56 m/s, diferença representando 43% da abordagem clássica. Estas diferenças encontram-se correlacionadas com a idade e a esbeltez das ondas.

Abstract of Dissertation presented to COPPE/UFRJ as a partial fulfillment of the requirements for the degree of Master of Science (M.Sc.)

THE IMPACT OF WAVE-MODIFIED WIND STRESS IN AN OCEAN CIRCULATION MODEL - APPLICATION TO THE SOUTH ATLANTIC

Nicolas Germain

January/2017

Advisor: Afonso de Moraes Paiva

Department: Ocean Engineering

A wave-related momentum flux parametrization is introduced in the ocean circulation model HYCOM. The physical process driving this parametrization is the growing and dissipation of the surface wave field. Two numerical experiments are conducted for the South Atlantic: one with the new wave effect included and a control run (without any wave information) used as a reference for comparison. The forcing fields (including the wave-modified ones) are produced based on ECMWF ERA-20C reanalysis data. A temporal and spatial characterization of surface stress under wave effects shows, in the mean, a lesser momentum flux for the whole domain (stress difference of -7%). Positive departures (wave-modified surface stress larger than the classic approach) are found during intense storm events mainly in the Southern region of the domain (up to +59% of stress difference). The long-term ocean response to the stress difference shows a strong SST signature in two particular areas: the Brazil-Malvinas confluence (difference of -0.9°C) and the Benguela upwelling (up to +1.1°C difference). The differences in SST are consistent with both the physical processes being modified by the waves (e.g. the Benguela upwelling being weaker due to an increased local Ekman pumping / weaker surface stress) and with similar numerical studies. The wave-related physical processes responsible for positive events are illustrated during two storm events: one in the Southern part of the domain and a second near the Brazilian Southern coast. Strong positive surface current differences are registered with values up to 0.56 m/s, representing 43% of the classic current approach. The difference is found correlated to the wave-age and the wave slope.

# Contents

# List of Figures

# List of Tables

# Chapter 1

# Introduction

Ocean surface waves affect the upper part of the ocean for being the physical interface between the atmosphere boundary layer and the ocean Mixed Layer (ML). Their role as the medium for exchanges between those two earth compartments has been better understood only recently as outlined by BABANIN [1].

Several efforts have been made by the scientific community to describe the wave effects by various parametrizations since there is still no single theory fully describing waves. Among the various effects, one can mention the enhanced turbulence in the ocean upper part caused by breaking waves CRAIG e BANNER [2], the Stokes-Coriolis Forcing (SCF) due to the interaction between the wave-induced Stokes drift and the Coriolis action MCWILLIAMS e RESTREPO [3] or the Langmuir circulation cells resulting from the same Stokes drift but combined this time to the mean flow MCWILLIAMS e RESTREPO [3]. BABANIN e HAUS [4] explored the wave-induced mixing due to non breaking waves (originated in the high Reynolds numbers of the wave orbital motion). The sea-state modified drag coefficient has been described by JANSSEN [5] through the use of a non-constant (sea state dependant) Charnock coefficient. Distribution of wind-induced momentum between the wave field and the ocean has been formulated by the European Centre for Medium-Range Weather Forecasts (see ECMWF [6]).

A natural next step has been to use the results of these wave parametrizations to study their effects on Ocean Circulation Models (OCM). At a regional scale, ZHANG *et al.* [7] studied the effect of wave-modified drag coefficient and bottom friction in the South China Sea and showed an increase of surface current of up to 0.4 m/s during a Monsoon storm event. DENG *et al.* [8] implemented the wave-induced Stokes-Coriolis forcing in three different ocean models (Global oceans at low resolution and South China Sea and Western North Atlantic ocean at higher resolutions) and found that Sea Surface Temperature (SST) and Mixed-Layer Depth (MLD) were noticeably influenced by the SCF.

The considerable advance in Wave Generation and Propagation Models (WGPM)

and the augmentation of computational capacities in major weather forecast centres allowed to study wave effects at larger scales and in coupled models. BABANIN *et al.* [9] showed the importance of the wave effects on a climate model of intermediate complexity using parametrizations for mixing of breaking waves, non-breaking waves and Langmuir circulation. BREIVIK *et al.* [10] explored the importance of three major wave effects (wave-modified surface stress, turbulent kinetic energy flux from breaking waves and the Stokes-Coriolis force) in forced and coupled experiments for a global (earth) system over a 30-years re-analysis period.

The wave-driven processes influence the vertical structure of the upper ocean (temperature in the mixed-layer and especially the upper few meters); and the distribution of the momentum flux and thus the surface current fields and finally the global circulation. This is of importance for basin scale modelling, e.g. influencing the Brazil Current transport. This has in its turn a potential impact on mesoscale processes such as vortices that are frequent in the Southeast Brazil. Even more locally, this has influence on the drift of floating objects and pollutants, which is of importance for oil spill modelling, search and rescue and dispersion of biological material.

Our main goal is to study the influence of wave effects on the parametrization of momentum fluxes at the air-sea interface in the South Atlantic and the consequences on an ocean circulation model for this same area. This main objective is divided in two main tasks which are:

- Data analysis of the momentum flux forcing fields: comparison of classic and wave-modified surface stresses
- Influence of wave-related parametrization on the ocean circulation model HYCOM: comparison of two model experiments, one without wave effect (classic approach) to a second one with wave-dependant surface stresses.

To do so the momentum flux parametrization of the ECMWF has been used (see ECMWF [6]) for the wave-influenced surface stresses. All necessary information (for classic approach and wave-dependant fluxes) are obtained downloading the ERA-20C reanalysis data. [1] We have used a one-degree resolution HYCOM model (BLECK *et al.* [11]) integrated over a decade, between 2001 and 2010 (after spin-up), for the numerical model study.

We have focused on the South Atlantic region with particular interest in three areas, highlighted throughout this document: The Southern Westerlies area, known

[1] http://www.ecmwf.int/en/research/climate-reanalysis/era-20c [accessed 2016/12/03]

for intense winds and strong storm activity, also forming the Southern bound of the South Atlantic gyre; the Trade wind area, characterized by constant winds and forming the upper limit of the above mentioned gyre; and the Southeast Brazil area, an economically active area (offshore petroleum industry, fishery, tourism) where lies the intense Western boundary Brazil Current. The global region and the three specific areas are shown in figure 3.1.

This thesis document has been written in an as concise as possible way and following the classical structure of an article. The material not considered of fundamental importance for understanding and more dedicated to deepen a particular subject or for illustration is presented in appendixes. The thesis is organized as follows. Chapter 2 describes the theoretical background of the physical processes leading to the two parametrizations used in the HYCOM model. Chapter 3 describes practically how the forcing fields are produced based on ERA-20C reanalysis data (POLI *et al.* [12]) and gives a spatial and temporal characterization of the wave-induced effect. Chapter 4 presents the HYCOM model set-up, the long-term results, extreme events study and results at a smaller time-scale (single events study). Chapter 5 discusses the results comparing them to climatological data bases and to other numerical experiments for single events study. The wave-age dependency of momentum flux transfer is also discussed. Chapter 6 concludes and makes suggestions for future works based on the identified limitations of the presented model set-up and the parametrizations introduced.

# Chapter 2

# Theoretical background - Wave effects in the Ocean Surface Boundary Layer

## 2.1 Energy/momentum transfers during waves generation and dissipation

Ocean surface waves act as a medium between atmosphere and ocean. They absorb energy and momentum from the atmosphere (wind field) as they grow and release energy and momentum when they brake, see BREIVIK *et al.* [10]. We can define $\tau_a$ the air-side stress (on the atmosphere side), $\tau_w$ the stress going to the wave field, and $\tau_{ds}$ the momentum flux released by the wave field to the ocean by breaking.

It is to be noted (see chapter 9.2 in BABANIN [1]) that the air-side stress is generally split into two parts: a viscous stress $\tau_{smflw}$ (also named tangential stress), which acts directly on the mean flow of the ocean upper part regardless of the wave field presence, and a turbulent part, which is absorbed by the waves ($\tau_a$). The smooth flow effect is generally negligible except for very low wind speeds (see classic drag coefficient curves in Appendix B.4). Another distinctive feature of the wave-supported energy transfer scheme is its ability to store and transport energy. Indeed the wave field transport energy away from its generation area at the group velocity $c_g$. The probably best known example is the breaking on the coast line of the swell which has been generated hundreds to thousands of kilometres away.

The resulting ocean stress (transferred to the ocean upper part) is named $\tau_{ocean}$ and is the sum of the viscous part and the momentum flux released by the wave field. In a fully developed sea state, waves are in equilibrium and do not take

energy any more from the atmosphere. All the momentum absorbed by waves is released via breaking (and other mechanisms) and in that case $\tau_a \approx \tau_{ocean}$. In the classic approach of surface stress (as described in section 2.3), the later situation is assumed happening all the time and the wave field is ignored. In the methodology described by BREIVIK *et al.* [10], the wave field effects are accounted for as described in section 2.4. Figure 2.1 illustrates this momentum flux modification (wind stress) for the two situations previously described.

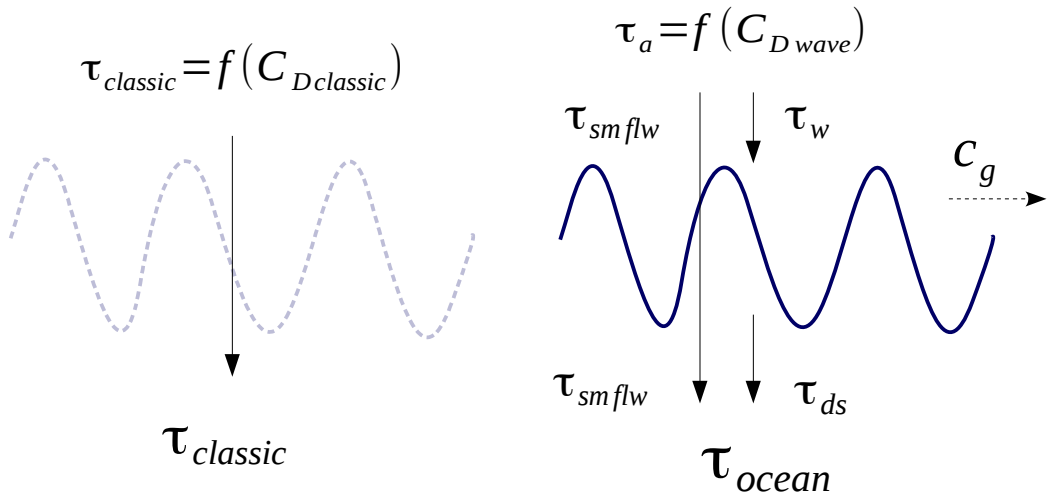


Figure 2.1: Air-sea momentum fluxes in the absence of wave information (left) and considering the wave field (right). The classic approach directly transfers the total classic stress, $\tau_{classic}$ (function of the classic drag coefficient) to the ocean. The wave-modified approach splits the atmosphere-side stress $\tau_a$ (function of the wave drag coefficient) into a smooth flow part $\tau_{smflw}$ and a wave-input part $\tau_w$. The smooth flow directly acts on the ocean and adds up with the wave dissipated part, $\tau_{ds}$, "given back" by the wave field through wave breaking, to form the total ocean-side stress $\tau_{ocean}$. The mean wave momentum flux $\tau_w$ is advected at the group velocity $c_g$.

## 2.2 Wave generation and propagation models of third generation

Third generation spectral wave models solve the wave action density $N$ (variance density spectra, or energy spectrum $F$ over the intrinsic frequency $\sigma$) without any assumption on spectrum shape. $N$ is a function of the wave number $\boldsymbol{k}$ and the wave direction $\theta$. The wave propagation is described by:

$$\frac{DN}{Dt} = \frac{S}{\sigma} \tag{2.1}$$

where $N$ is the wave action density previously defined, $D/Dt$ is the total derivative, $\sigma$ the relative (intrinsic) frequency (as seen by an observer moving with the current) and $S$ is the effect of the source and sink terms. The variance density spectra $F$ can be related to the wave group velocity $c_g$ mentioned in figure 2.1, re-writing equation 2.1 in flux form (it can be found in BREIVIK *et al.* [10]).

In deep water, $S$ is generally considered as the sum of three components: $S_{in}$ the wind-wave interaction term, $S_{nl}$ the non-linear wave-wave interaction term and $S_{ds}$ a dissipation term (due to wave breaking).

## 2.3 Classical surface stress computation

Ocean surface stresses due to the action of wind were suggested to be related to the friction velocity $u_*$ and a drag coefficient $C_D$ by G. I. Taylor in 1916 as recalled by STULL [13]:

$$u_*^2 = C_D U^2 \tag{2.2}$$

with $U$ the mean wind speed at a specified height. The log-wind profile derived from the similarity theory allows to relate $C_D$, the measurement height $z$ and the surface roughness $z_0$. We have, for a statically neutral condition in the surface layer:

$$C_D = \frac{\kappa^2}{ln(z/z_0)^2} \tag{2.3}$$

Here $\kappa$ is the Von Kármán constant, taken equal to 0.4. CHARNOCK [14] gave a relation for the surface roughness $z_0$ on a water surface based on the friction velocity,

$$z_0 = 0.015\,\frac{u_*^2}{g} \tag{2.4}$$

The coefficient 0.015 in equation (2.3) is called the Charnock constant. The three equations previously introduced allow to estimate the friction velocity and the drag coefficient based on the wind speed in an iterative process for neutral conditions. In non-neutral conditions, some additional terms in the drag coefficient equation are necessary to account for the stability of the lower part of the atmosphere.

From the resolved scheme above, one can derive the surface stress $\tau_{classic}$ based on:

$$\tau_{classic} = u_*^2\,\rho_a \tag{2.5}$$

where $\rho_a$ is the air density.

The surface stress derived in that way does not have any information from sea state and can be seen as an air-side stress as well as the stress going to the ocean. This is the classical approach as illustrated in the left part of figure 2.1 and which is widely used in ocean modeling.

## 2.4 Wave-modified stress

In equation 2.4, the surface roughness depends only on the friction velocity and gravity and brings no modification from the sea state. JANSSEN [5, 15] assumed a non-constant Charnock coefficient $\alpha_{CH}$, depending on sea-state:

$$\alpha_{CH} = \frac{0.006}{\sqrt{1 - \tau_w/\tau_a}} \tag{2.6}$$

where $\tau_a$ and $\tau_w$ are the stresses described at the beginning of this chapter. This parameter replaces the constant coefficient (0.015) of equation 2.4.

This leads to a new, wave-modified, drag coefficient $C_{D\,wave}$ associated to the air-side stress ($\tau_a$) which accounts for the sea state. This is done in a loop process (within the wave model resolving scheme) since $\tau_a$ appears as input and output. This is what we will call through this document the **first wave effect**.

Recalling the stress distribution presented in figure 2.1 (right-hand side) and following ECMWF [6], the resulting ocean stress is equal to the air-side stress minus the stress absorbed by the wave field (positive) minus the stress injected by the wave dissipation (negative):

$$\tau_{ocean} = \tau_a - \tau_w - \tau_{ds} \tag{2.7}$$

This is the **second wave effect**. Note that the smooth flow effect does not directly appear in this equation but is included in the air-side stress and thus in $\tau_{ocean}$ as can be seen in the figure 2.1.

The stress components $\tau_a$, $\tau_w$ and $\tau_{ds}$ are related to the source terms of equation (2.1) and are computed by the wave generation and propagation model.

# Chapter 3

# Surface stresses data analysis

We present, quantify and discuss the differences between the two approaches (classic stress versus wave-modified stress) in order to characterize spatially and temporally the wave effects and the physical processes at play. We seek to characterize the global wave influence as well as the contribution of each one of the two effects previously presented: the wave-modified drag coefficient and the momentum flux modification through the wave field.

## 3.1 ERA-20C climate reanalysis

ERA-20C is an atmospheric reanalysis of the 20th century with assimilation of observed surface pressure and surface marine winds, see POLI *et al.* [12]. It has been produced by the ECMWF. A climate reanalysis is a numerical description of the recent climate, produced by combining models (land, wave and atmosphere in our case) with observations based on a single version of a numerical forecast system.

ERA-20C has been selected since it freely provides all the necessary data to force our two experiments. Data are available for download on ECMWF website either *manually* or in a *programmatic way* (web API). Forecast data of the wave and atmospheric models have been used at a 6 hours frequency.

We shortly describe now the production of the forcing fields. Only stress-related fields are discussed, the remaining ones (wind speed, moisture, temperature, precipitation and radiation fluxes) being presented in appendix C.1. The necessary parameters (downloaded from ERA-20C database) are the following: 10-meter neutral wind $U_{10}^n$, the wave-modified drag coefficient $C_{D\,wave}$, the mean sea level pressure $p$, the 2-meter dew point temperature $T_{dp}$ and the normalized stress into ocean coefficient $\widetilde{\tau}$ (see equation 3.3).
Following equation (3.27) of ECMWF [6], one can derive the air density over ocean $\rho_a$ from $p$ and $T_{dp}$ as follow:

$$\rho_a = p \,/\, (R\, T_{dp}) \tag{3.1}$$

with $R$ a gas constant for dry air (in $J\,kg^{-1}K^{-1}$). The 10-meter neutral wind relates the (neutral) drag coefficient to the actual surface stress (acting for any stability condition) as described in ECMWF [16]. The wave-modified surface stress is then computed combining equations 2.2 and 2.5:

$$\tau_a = \rho_a \, C_{D\,wave} \, U_{10}^{n\,2} \tag{3.2}$$

The stress going to the ocean $\tau_{ocean}$ is obtained from the air-side stress and the normalized stress into ocean coefficient:

$$\tau_{ocean} = \widetilde{\tau} \, \tau_a \tag{3.3}$$

Where $\widetilde{\tau}$ is not given by the wave model (over ice, or where the grids do not match near shore), the classic stress is used to force our models. To compute the classical surface stress, we need a (neutral) drag coefficient $C_{D\,classic}$ from a bulk formula that we find in RENFREW *et al.* [17]. The classic surface stress is then computed as follow:

$$\tau_{classic} = \rho_a \, C_{D\,classic} \, U_{10}^{n\,2} \tag{3.4}$$

Further details on the two drag coefficients used for the first wave effect are given in appendix B.4 together with a comparison with NOAA NCEP/CFSR formulation.

## 3.2 Global effect (both wave effects)

We present here a spatial and temporal characterisation of the wave effects on the momentum flux. We present maps of the absolute difference $\tau_{ocean} - \tau_{classic}$ (in $N/m^2$) of surface stresses and of the relative difference $(\tau_{ocean} - \tau_{classic})/\tau_{classic} * 10^2$ (in % of the classic stress approach) and scatter plots of the stress ratio $\tau_{ocean}/\tau_{classic}$. Overall, we see a diminution of the surface stress under wave influence with positive departures of positive difference (wave-modified stress larger than the classic approach). We explore then the relative importance of each of the two wave effects presented in the previous chapter, i.e. the drag coefficient modification ($1^{st}$ effect) and the momentum fluxes distribution ($2^{nd}$ effect). The first effect is the one responsible for most of the total effect (combination of the two effects).

### 3.2.1 Mean and RMS difference maps

Figure 3.1 shows the mean relative stress difference and the relative Root Mean Square (RMS) stress difference for the period 2001-2010, expressed in percentages of the mean classic stress (difference and RMS difference formulae are defined in

the figure legend). The left part is a measure of the mean effect (panel a) while the right one quantifies the variance of the global effect (panel b). The wave mean effect is to reduce the stress (space-averaged value is -6.7% for the full domain) with a significant variability over the domain (RMS difference is 12% for the entire area). The mean relative difference is significantly smaller in the Southern Westerlies area, -3.3%, due to a relatively small absolute value difference (-0.008$N/m^2$) combined to a hight mean stress (0.25$N/m^2$). Similarly, the low absolute values for the African West coast (both mean and RMS difference are close to zero) influence greatly the exagerated relative difference and RMS difference shown in figure 3.1.

Regarding the distribution of stress absolute values (in $N/m^2$, presented in figures A.1 and A.2 of appendix A.1), one can mention a stronger difference following a diagonal linking the South Africa tip to the Brazilian Northeast region with a regional extreme of -0.011$N/m^2$ for the Trade winds area (see figure A.2). The Southern Westerlies area shows the biggest absolute RMS difference (0.03$N/m^2$, about three times the value of the other two areas), a specificity less visible when we first looked at the relative RMS difference. This large absolute value is highly correlated to the intense wind stress found in this area (see figure A.1).

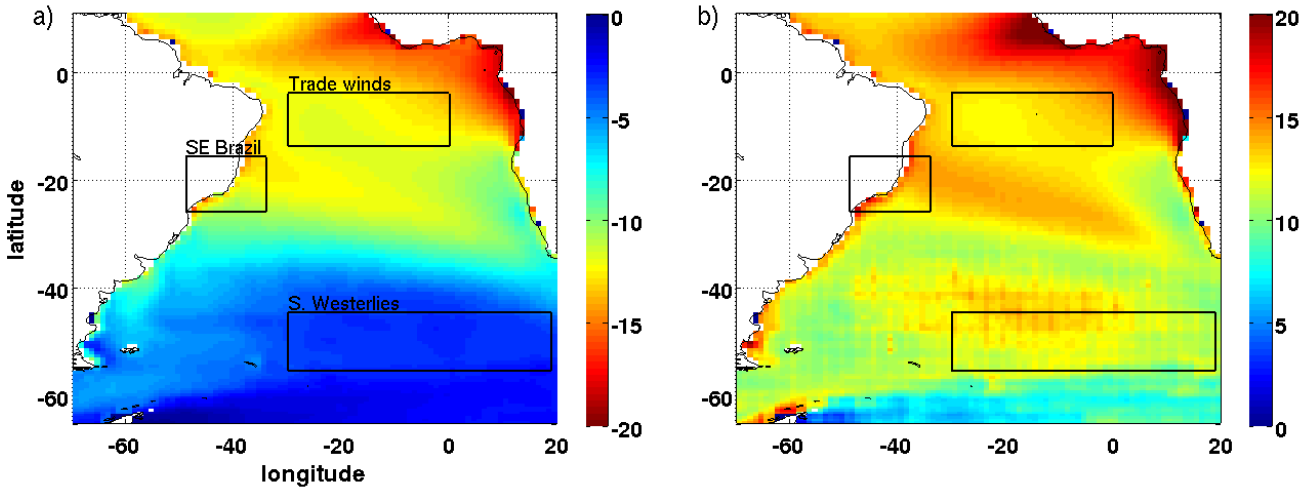


Figure 3.1: **Panel a**: Relative difference of mean classic stresses, in % of mean classic stress, i.e. $(\overline{\tau_{ocean}} - \overline{\tau_{classic}})/\overline{\tau_{classic}} * 10^2$ , where the over bar symbol denotes the (time) average for the period 2001-2010. The space-averaged values are -6.7% for the full domain, -3.3% for the Southern Westerly area, -12% for the Trade winds area and -12% for the SE Brazil area. **Panel b**: Relative Root Mean Square stress difference, in % of mean classic stress, i.e. $\sqrt{1/N * \sum(\tau_{ocean} - \tau_{classic})^2}/\overline{\tau_{classic}} * 10^2$, with $N$ the number of observations for the same period. The space-averaged values are 12% for the full domain, 12% for the Southern Westerly area, 13% for the Trade winds area and 14% for the SE Brazil area. Note the colour scale inversion between the two panels.

### 3.2.2 Stress ratio scatter plot

The total effect of wave influence can be seen in figure 3.2 for the total domain and for each of the three areas shown in figure 3.1. A stress ratio $\tau_{ocean}/\tau_{classic}$ greater than one means a wave-modified stress stronger than the classic approach. We find the same behaviour for the above ratio than for the relative difference of section 3.2.1: a mean effect with a lesser wave-modified ocean stress. The domain-wide mean ratio is 0.89 with a standard deviation of 0.07. Positive events are globally rare, accounting for 2.7% for the full domain but up to 12% for the Southern Westerlies area. They are marginal for the Southeast Brazil area (0.06%) and totally absent for the Trade winds area. All areas display a clear tendency: the stronger the wind, the stronger the ratio, with positive correlation coefficients (see the correlation table 3.1). The Southern Westerlies area has positive events no matter the wind intensity value, though the 5-15 m/s wind range has less extreme ratios compared to the remaining wind intensities. The variance of the effect seems to mostly come from the Southern Westerlies area, with a relation between variance and the wind intensity. Indeed the Southern area has the most intense winds (see the blue curves of classic wind stress) and the positive events (bringing the variability) for winds above 10 m/s represent 9.5% out of the previously mentioned 12%.

## 3.3 Two effects comparison

One can ask what is the relative importance of each of the two effects described in section 2.4. Figure 3.3 allows us to evaluate this relative influence for the entire domain. The stress ratio for each effect is plotted in the same fashion than for both effects as in previous section (ratios definition given in the figure legend). In the mean, the first effect ratio, the drag coefficient modification, equals 0.89 (standard deviation of 0.08) while the second, the momentum fluxes modification, is 0.99 with a slightly smaller standard deviation (0.06). This is consistent with BREIVIK *et al.* [10] who bears responsible the first effect for most of the origin of the total mean effect. Indeed the total mean effect ratio is also equal to 0.89 (as the $1^{st}$ effect) and the $2^{nd}$ effect ratio is close to unity (0.99), thus not influencing the total mean effect ratio. This is confirmed by a higher (linear) correlation between the first and the total effects (0.78 for the entire domain) than between the second and total effects (0.19).

One striking feature of the comparison is the anti-correlation between the two effect tendencies: while the first one has a positive slope (linear correlation with the 10m wind is 0.90), the second effect tends to decrease while the wind speed increase (negative correlation with wind: -0.40). Those opposite slopes explain the two peaks

of positive events of the figure 3.2 (upper left panel) and the sparse zone (less dense) above a ratio of approximately 1.2 in the wind range 5-15 m/s.

The second effect is positive 22% of the time for the region-wide area, while the first one is only positive 4.2% of time. Positive events are more frequent for both effects in the Southern area although with a lesser asymmetry between the two effects: 16.3% for the first effect and 34.6% for the second one (see figure A.3 in appendix). The first effect is rarely positive for the two other areas (Trade winds and SE Brazil), with a frequency lower than 1%. All areas have the same anti-correlated behaviour and the Southern Westerlies area is once again responsible for most of the variability of the entire domain.

## 3.4 Partial conclusion on stress difference

We have seen that, globally, the mean wave effect is a slightly weaker wave-modified ocean stress (than the classic approach) with occasional positive events (i.e. $\tau_{ocean} > \tau_{classic}$). The Southern Westerlies area contrasts with the other areas for hosting the majority of the positive events. Those positive events are responsible for the wave effect variability: strong in the Southernmost area (probably linked to the intensity of wind stress found in this region) and far weaker in the other areas.

The first wave effect comes from the increased sea surface roughness due to the presence of growing (short) waves. Practicallly, the difference between the classic approach ($\tau_{classic}$) and the wave-modified drag coefficient (producing $\tau_a$) comes from the parametrization retained for the Charnock coefficient (see equation 2.4): either constant (classic approach) or wave-dependant (equation 2.6). Further details can be found in ECMWF [6] and in appendix B where the ECMWF coupling scheme is shortly presented and specific results for the Southern Atlantic are shown for the absorption ratio ($\tau_w/\tau_a$), the wave-modifed Charnock coefficient and for various drag coefficient formulations ($C_D$).

The second wave effect can be seen as a buffer for energy, either retaining it (wave growing situation) or giving it back (wave dissipation). Once again the parametrizations used in the ECMWF wave model (WAM, see ECMWF [6]) for dissipation and wave growth (see equation 2.7) are responsible of the practicle numerical results. The potential links between wave physical parameters and this second wave effect are explored in sections 4.3 and 4.4.

The mild mean wave effect can be explained as follow: on the average, wave growth and dissipation are close to an equilibrium. This is reflected by the wave age ($c_p/U_{10}^n$) [1] being most of the time close to 1.2 (see figure 3.4), denoting a fully developed, mature sea (see EDSON *et al.* [18]). This fully developped sea is related

[1] $c_p$ is the wave phase speed as derived from the linear theory of waves

to a wave-modified Charnock coefficient slightly lower than the classic approach (0.011 and 0.018 respectively, see appendix B.3) and thus a slightly smaller roughness length for the wave-modified case. This explains why the first effect is of moderate intensity and giving a slightly lower wave-modified surface stress. The second effect is nil in case of equilibrium between wave growth and dissipation as shown by equation 2.7 and the total effect is in that case depending on the first effect only.

Another interesting feature is the fact that the two effects are anti-correlated and partially compensate each other, softening the global effect towards the no-wave-effect situation. Indeed, an increased wave-modified drag coefficient (increased wind stress) would be compensated by a lesser ocean-side stress, originated in either a growing sea (retaining energy) or a developed sea where local energy propagate elsewhere as swell. This mutual compensation is a weak effect, as shown by the low anti correlation coefficient between the two effects (-0.46 for the entire domain). This compensating effect is stronger for the two Northernmost areas (correlation near -0.75) and weaker for the Southern Westerlies area (-0.48). All correlation coefficients are recalled in the table 3.1.

The inversion of sign for the second effect correlation with the total effect between the full area plus the Southern W. area (positive correlation) and the Northern areas (negative $R^2$) is another interesting point and can be interpreted as follow: in mild conditions (Northern areas, lowest cells) the second wave effect occurs at low wind speed and the second effect is opposite to the global effect (reservoir effect). While for the Southern Westerlies area the stronger winds make the wave break at the time of heavy sea conditions (saturation of energy input into the wave field) therefore contributing positively to the total effect (positive correlation).

| $R^2$ | Total effect | | $1^{st}$ effect | | $2^{nd}$ effect | |
|---|---|---|---|---|---|---|
| Wind | 0.71 | 0.42 | 0.90 | 0.80 | -0.40 | -0.45 |
| | 0.84 | 0.83 | 0.97 | 0.95 | -0.77 | -0.71 |
| Total effect | | | 0.78 | 0.60 | 0.19 | 0.42 |
| | | | 0.89 | 0.91 | -0.39 | -0.34 |
| $1^{st}$ effect | | | | | -0.46 | -0.48 |
| | | | | | -0.77 | -0.70 |

Table 3.1: Linear correlation coefficients between the following variables: Wind (10-m neutral wind), total wave effect ($\tau_{ocean}/\tau_{classic}$), $1^{st}$ wave effect ($\tau_a/\tau_{classic}$) and $2^{nd}$ wave effect ($\tau_{ocean}/\tau_a$) . Coefficients are given for the full domain, Southern Westerlies area, SE Brazil area and Trade winds area (clock-wise starting upper left) in sub-cells for each variable combination.

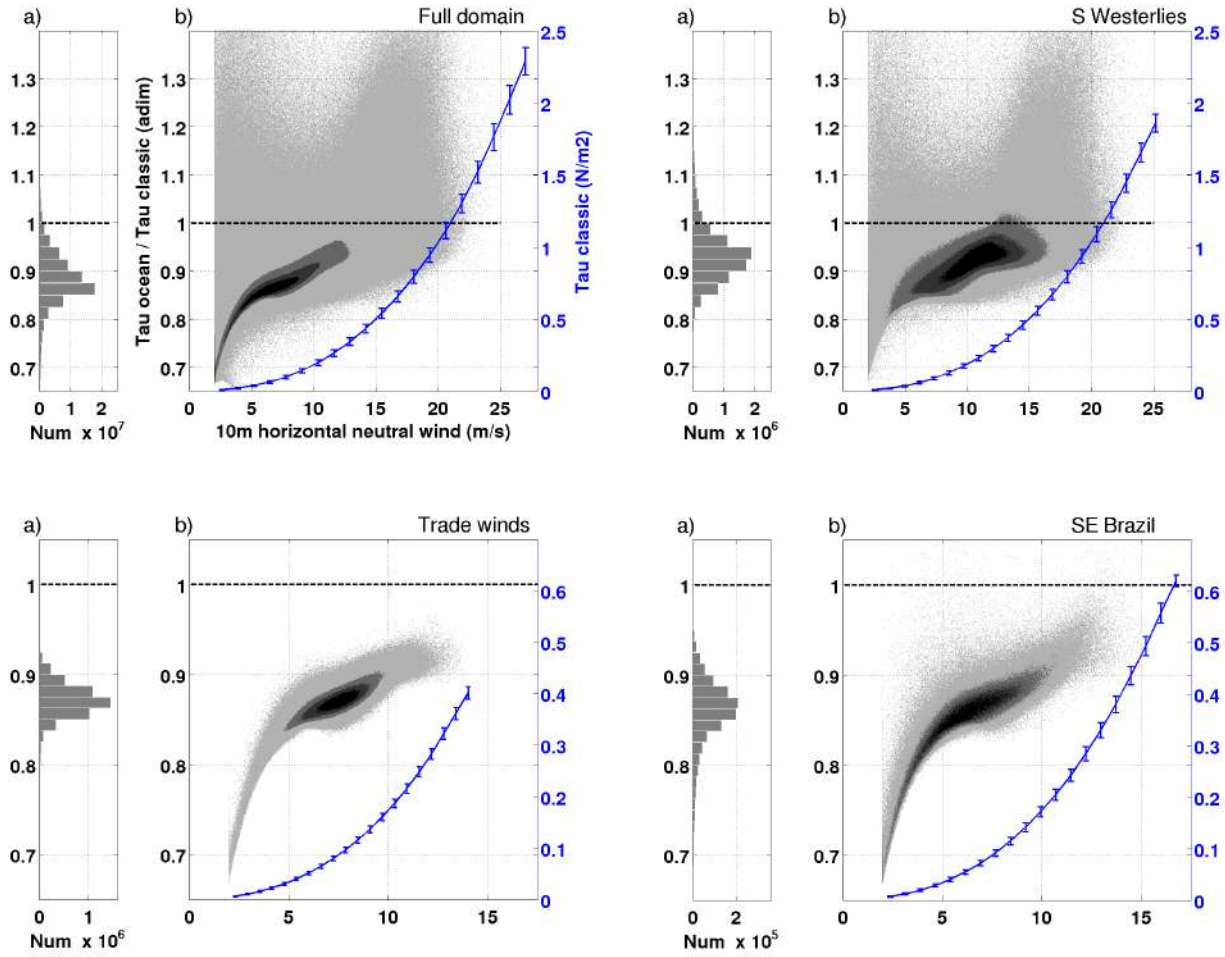


Figure 3.2: Stress ratio $\tau_{ocean}/\tau_{classic}$ (grey tones, dimensionless), and classic stress (blue in $N/m^2$) for the 2001-2010 period. **Four areas** are presented: Full domain, Southern Westerlies, SE Brazil and Trade winds (clockwise, starting from top left). Each area is composed of **Panel a**: Stress ratio distribution (in number of occurrences for the area) for ranges of ratio. **Panel b**: Scatter data of the ratio plotted against the 10m neutral wind, where each tone of grey represents 25% of the total amount of information (space x time) and a darker grey is a more frequent ratio (4 tones used). The blue curve is the mean classical stress $\tau_{classic}$ with the vertical bars representing two standard deviations of the distribution. Note the difference of scales between the upper and lower panels.

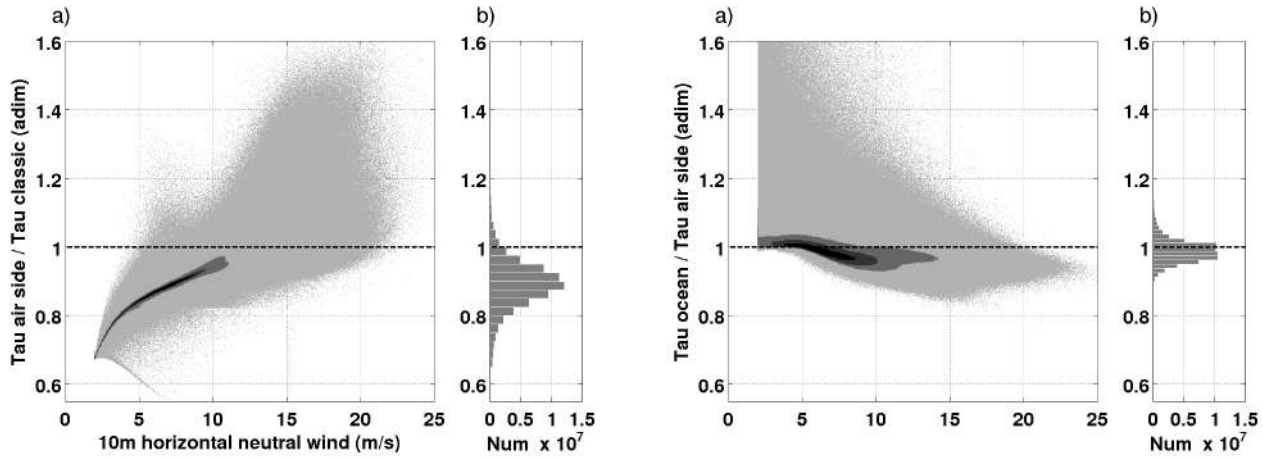


Figure 3.3: Stress ratio for the **two wave effects**: Left panel is $\tau_a/\tau_{classic}$ and right panel is $\tau_{ocean}/\tau_a$ for the 2001-2010 period and considering the full domain. **Panel a**: Scatter data of the ratio plotted against the 10m neutral wind, where each tone of grey represents 25% of the total amount of information (space x time) and a darker grey is a more frequent ratio (4 tones used). **Panel b**: Stress ratio distribution (in number of occurrences for the area) for ranges of ratio.

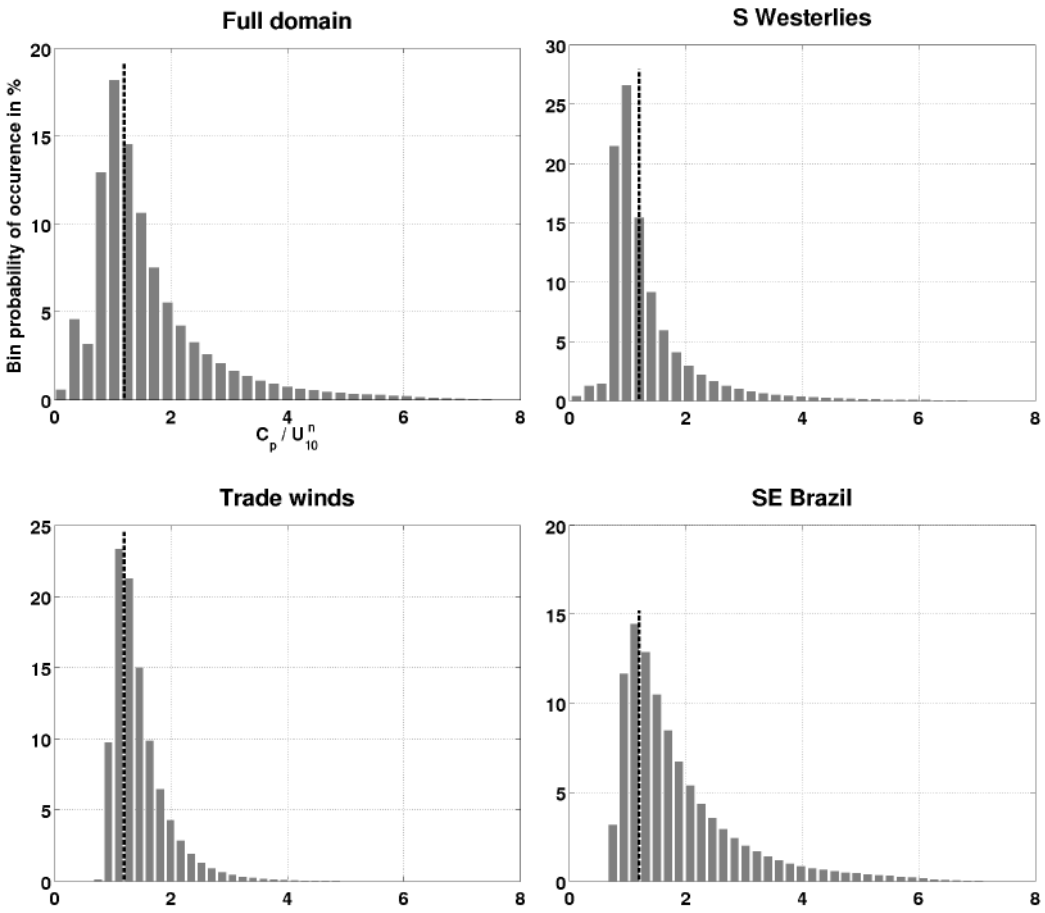


Figure 3.4: Wave age distribution, i.e. histogram of $c_p/U_{10N}$ for the various areas considered: Full domain, Southern Westerlies, SE Brazil and Trade winds (clockwise, starting from top left). Each bin contribution is given in % of the total number of observations, the sum of all bins being 100%. The vertical doted line is the 1.2 limit recalled in EDSON *et al.* [18] defining mature fully developed seas. A smaller than 1.2 wave age corresponds to a young developing sea and a greater than 1.2 corresponds to an old (decaying) sea state.

# Chapter 4

# HYCOM ocean circulation model experiments

Now that we have characterized the variations in the wind stress forcing fields, we can focus on the HYCOM model results. We first present a short description of the model set-up and some general results allowing us to validate the global behaviour of the model. The mean wave effect is then explored analysing averaged quantities at the basin scale and linking their differences to the results of the chapter 3. We finally focus on two extreme storm events and their impact on the surface current.

## 4.1 Model set-up

We have used a 1° resolution staggered-grid to model the South Atlantic region in the HYbrid Coordinate Ocean Model (BLECK *et al.* [11]). The model extends meridionally from 65°S to 11°N and zonally between 70°E to 20°W (see GABIOUX [19]). 21 hybrid layers are used for the vertical discretization (see table 4.1) and the bathymetry is interpolated from ETOPO2 dataset. [1] Relaxation is done monthly based on the World Ocean Atlas 2009, WOA2009 (ANTONOV *et al.* [20], LOCARNINI *et al.* [21]), for temperature and salinity at open boundaries of the domain with a 5 to 30 days e-folding time scale over 3 degrees horizontally (see PAIVA *et al.* [22]). Barotropic forcing (lateral boundary nudging) is done for the two major currents acting in the Southern region: the Antarctic Circumpolar Current (ACC) - entering the domain at the Drake strait and exiting at Good Hope cape - and the Agulhas current (entering at the cape of Good Hope). Their respective transports are 120 Sv (ACC West), 110 Sv (ACC East) and -10 Sv for the Agulhas current (taken from GABIOUX [19]).

[1] National Geophysical Data Center, 2006. 2-minute Gridded Global Relief Data (ETOPO2) v2. National Geophysical Data Center, NOAA. doi:10.7289/V5J1012Q [accessed 2016/11/02].

| Layer | $\sigma_\theta$ | Water masses | Thermohaline Index |
|---|---|---|---|
| 1 | 19.5 | layers used for a finer discretization of the mixed layer | |
| 2 | 20.25 | | |
| 3 | 21 | | |
| 4 | 21.75 | | |
| 5 | 22.5 | | |
| 6 | 32.25 | | |
| 7 | 24 | | |
| 8 | 24.7 | | |
| 9 | 25.28 | **TW** or maximum of salinity Water (MSW) | T>20°C S>36.4 |
| 10 | 25.7 | **SACW** | 6°C<T<20°C 34.6<S<36.4 |
| 11 | 26.18 | | |
| 12 | 26.52 | | |
| 13 | 26.8 | | |
| 14 | 27.03 | **AAIW** | 3°C<T<6°C 34.2<S<34.6 |
| 15 | 27.22 | | |
| 16 | 27.38 | | |
| 17 | 27.52 | **NADW** | 3°C<T<4°C 34.6<S<35.0 |
| 18 | 27.64 | | |
| 19 | 27.74 | | |
| 20 | 27.82 | | |
| 21 | 27.88 | | |

Table 4.1: Vertical discretization in $\sigma_\theta$ layers for the one degree simulation. Column 3 indicates the water masses that are represented by each model layer (TW – Tropical Water; SACW – South Atlantic Central Water; AAIW – Antarctic Intermediate Water; NADW – North Atlantic Deep Water), and column 4 the thermohaline indexes for each water mass. Taken from GABIOUX *et al.* [23]

A 10-year initial spin-up period is ran with monthly climatological forcing from ERA-20C (averaged over 1996-2010). This information includes the wind speed, wind stress (classic formulation for spin-up), net thermal radiations (short and long waves), air temperature, specific humidity and precipitations (see PAIVA e CHASSIGNET [24]). The model is then forced with synoptic fields (6-hourly). Note that surface relaxation is always turned off (S and T) since a wave-effect signature is expected on the SST (see BREIVIK *et al.* [10]). Eleven years are run (2000 to 2010) and the first year is discarded. Two sets of forcing data are used producing two sets of results, with only the surface stress varying from one set to the other. The first control experiment, **CTRL**, is integrated using the previously defined surface stress $\tau_{classic}$ (equation 3.4) which does not include any wave information. The second experiment, **WAVE**, is forced with the total wave effect $\tau_{ocean}$ given by equation 2.7 and includes both wave effects defined in section 2.4, i.e. the wave-modified drag coefficient ($1^{st}$ wave effect) and the fluxes modification ($2^{nd}$ effect). The momentum flux parametrization used in each experiment is recalled in the table 4.2.

## 4.2 Large scale results

**Global behaviour**

The model reaches an equilibrium before the end of the first year of the spin-up

| Experiments | Momentum flux parametrization |
|---|---|
| **CTRL** | $\tau_{classic}$ equation 3.4 |
| **WAVE** | $\tau_{ocean}$ equations 3.2 & 3.3 |

Table 4.2: HYCOM experiments: definition of the wind stress forcing fields for the two runs. Note that the total wave effect (including both effects defined in chapter 2) is used for the WAVE experiment

period, as can be seen in the figure 4.1. Both CTRL and WAVE experiment results are plotted (after spin-up last year "sp10") and we see a slightly less energetic ocean for the later case, consistent with a globally smaller wave-modified surface stress, as outlined in chapter 3.2.1.

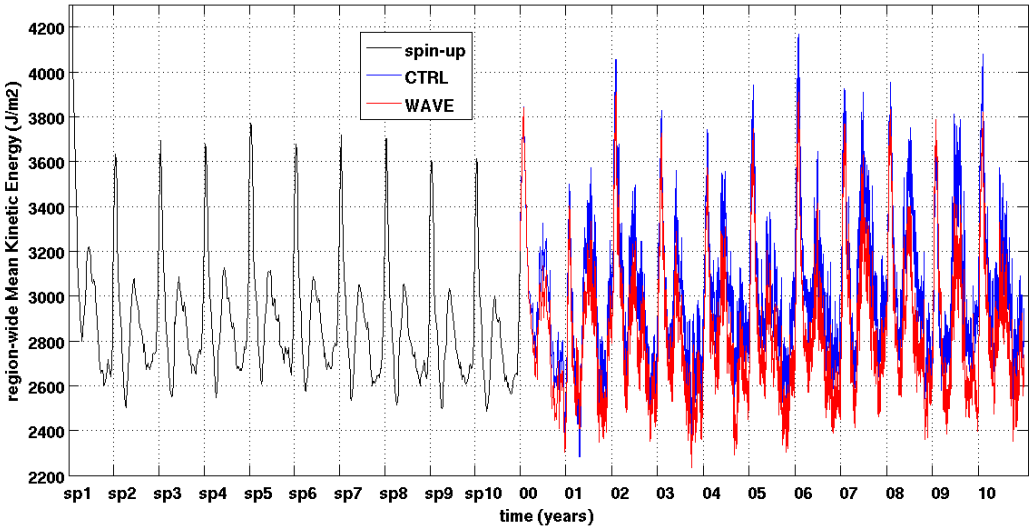


Figure 4.1: Time series of domain-integrated kinetic energy for the entire domain, considering three-dimensional velocity fields (in $J/m^2$), The spin-up period is labelled "sp1" to "sp10" and is sampled every 6 days. The CTRL (blue) and WAVE (red) synoptic runs are sampled 6-hourly (except for the first "00" year which is sampled as for spin-up) so the diurnal variability can be seen

The model mean fields compare well with the WOA2009 climatology, as shown in figure 4.2. The Antarctic Intermediate Water is reasonably represented in the upper 1500 m. Deeper structure (e.g. NADW) is less well represented due to the reference pressure used in HYCOM for the equation of state, taken at the surface (not shown). This is deemed of minor importance in our case since the wave effects are predominantly found in the upper 800 m for water masses structure. Figure C.6 in appendix shows a meridional section at 25°W clearly showing this behaviour, the

wave effects being restricted to the upper 800m, for the mean temperature and the mean salinity. The CTRL experiment general circulation is shown in the left panel of figure 4.3 and presents a well-defined South Atlantic gyre, with the maximum of SSH situated near 35W/25S. The Brazil Current (BC) intensity is used as a metric of the models ability to represent the South Atlantic gyre adequately. The mass transport of the BC is computed through an inclined section near 23S (section lon/lat end coordinates: 42W/22S and 39W/24S) following the method for transport integration from GABIOUX *et al.* [23] (later on referred to as [23, Gab]). The 10-year mean values are 5.4 Sv (std 3.3 Sv) for CTRL and 4.4 Sv (std 2.9 Sv) for WAVE. The classic approach (CTRL) is very close to the mean value computed in the 1/12° simulation of [23, Gab] (about 5 Sv), giving confidence in the new forcing data used (ERA-20C for our simulation where [23, Gab] used NCEP/CFSR) and the model behaviour. The WAVE experiment transport is weaker than the CTRL one, as expected. We find a reasonable agreement between those transport values and the literature review made by DA SILVEIRA *et al.* [25] and recalled in figure 7 of [23, Gab]. The seasonal (annual and semi annual) variability of the BC is well represented as can be seen in appendix C (figure C.5), together with additional results illustrating the global behaviour of the two HYCOM experiments. We can conclude at this point that the experiments perform well and form a solid basis for the intended purpose of comparison.

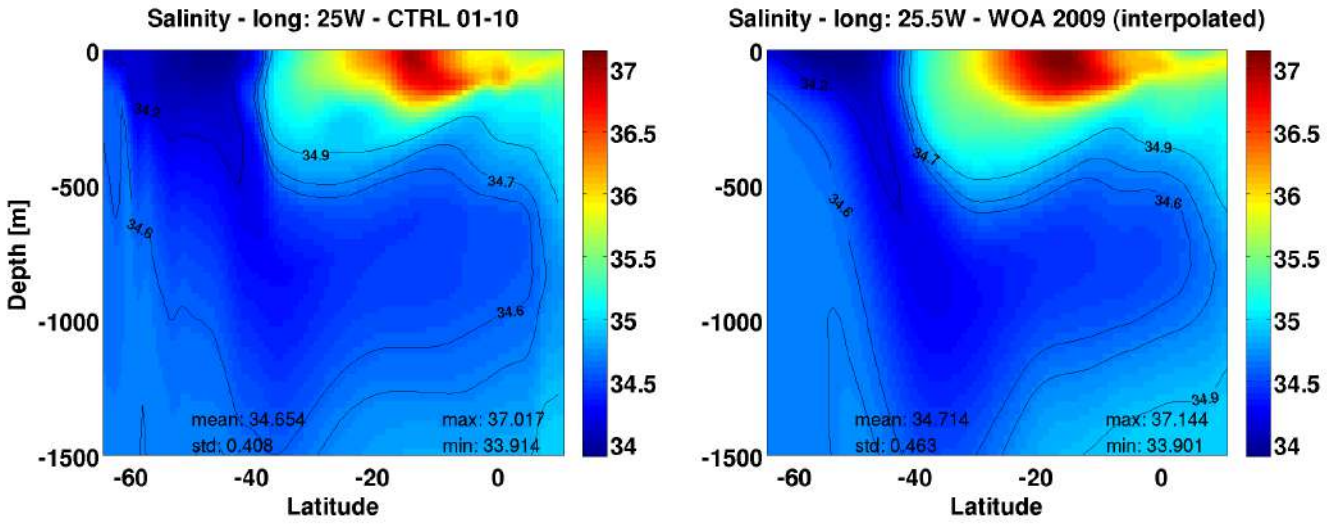


Figure 4.2: Meridional section at 25W of mean salinity (in psu) between surface and 1500m depth. **Left panel**: 2001-2010 mean value from HYCOM integration (CTRL run). **Right panel**: WOA 2009 climatology values interpolated on HYCOM grid. The salinity range 34.2-34.6 represent the AAIW, see table 4.1).

**Long term difference**

Figure 4.3 shows the long term results of mean values (CTRL run, left panels) and mean differences (right panels) for Sea Surface Height and Sea Surface Temperature. The main feature of the SSH difference is the global weakening of the South Atlantic gyre, as shown by the lowering of the SSH in the central Western part of the South Atlantic with differences up to -3.7 cm. This expected result originates in a weaker surface stress curl ($\nabla_h \times \vec{\tau}$) and consequently a weaker Ekman pumping. We show this result in figure 4.4. The Ekman pumping displays a clear weakening in the whole central South Atlantic. The Sverdrup meridional transport shown on panel b) is integrated from East (African West coast) to a Western limit located offshore the Brazilian coast for latitudes between 9°S and 32°S. It exhibits a consistent behaviour with the surface stress variation showing a weakening of the wave-modified situation (red) of up to 2 Sv (difference shown in the upper horizontal axis, in magenta).

Geographically, two extreme differences are seen in the Benguela upwelling area (positive difference) and near the Brazil-Malvinas confluence zone (negative difference), for both the SST and the SSH. The Benguela warmer upwelling (positive SST difference) is consistent with the positive Ekman pumping difference presented in figure 4.4 at the same geographical location. Indeed a smaller quantity of cold deep-water is brought to the surface leading to a weaker manifestation of the upwelling, i.e. a hotter singularity. The long-term mixed-layer depth in this region is deeper (positive difference) for the WAVE run (see figure C.7 in appendix). This can be explained by a weaker upward vertical velocity (downward Ekman pumping difference is positive in figure 4.4) allowing a deeper mixed-layer.

A cold signature of SST long term difference in the confluence area between the Brazil and the Malvinas currents is seen near 50W/32S. The weaker BC results in a smaller quantity of heat brought from the Tropics leading to the cold singularity. This is of major importance since the area is very active in terms of exchanges of mass, heat, and salt between the South Atlantic subtropical gyre and the Antarctic Circumpolar Current (see JULLION *et al.* [26]). It is also a subduction area where Subantarctic Mode Water is formed. This wave-modified colder singularity is somewhat counter intuitive with the weak shallowing of the Mixed Layer (ML) in the same area which is normally deeper than the surrounding area (see figure C.7 in appendix). One would normally expect from a shallower ML to be hotter. This emphasis the complexity of the regional dynamic.

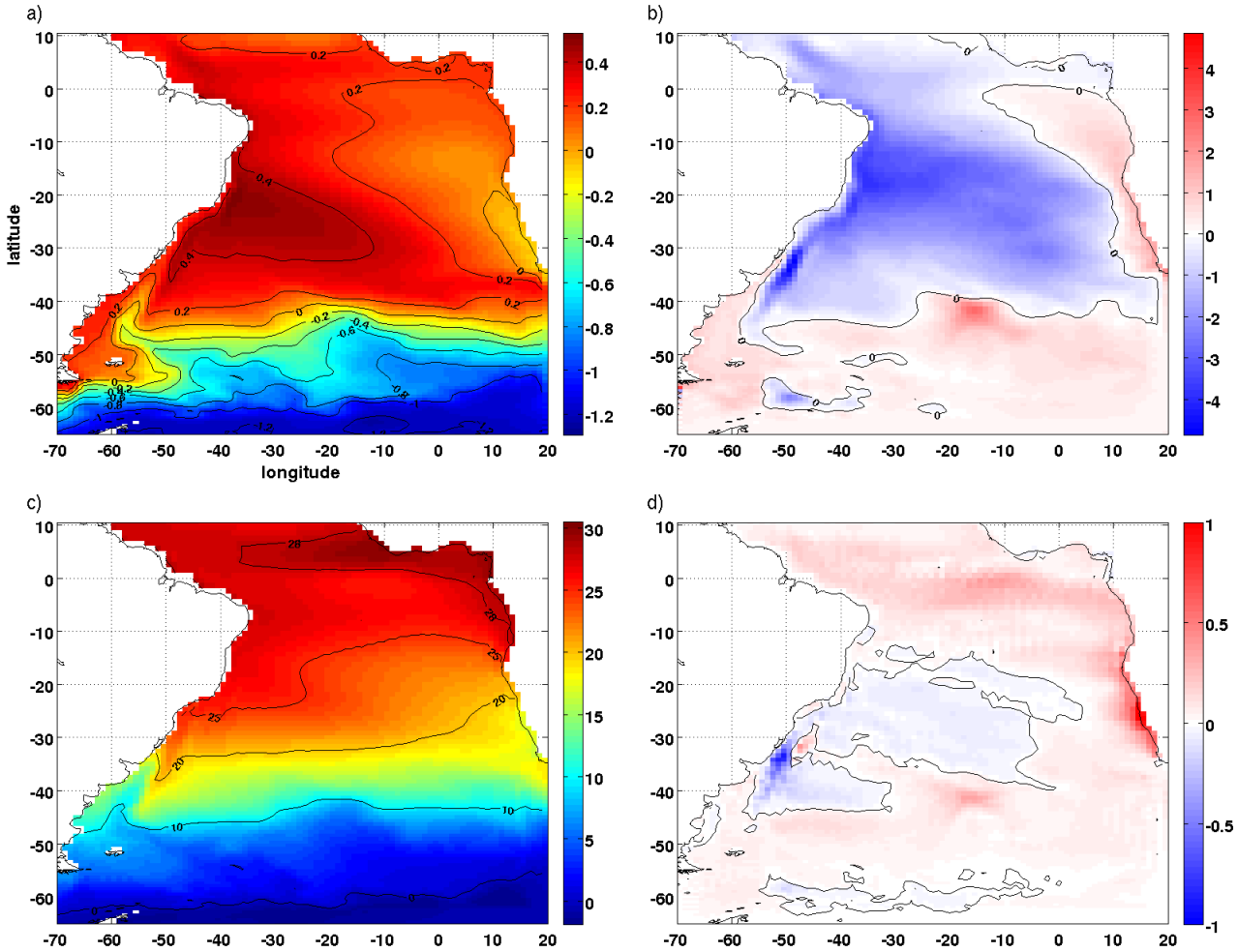


Figure 4.3: Long term results for SSH and SST. **Panel a**: mean sea surface height (in meters) over the period 2001-2010 for CTRL experiment. The **Panel b** is the long term difference of SSH between WAVE and CTRL runs, in centimetre, i.e. $\overline{SSH}(\tau_{ocean}) - \overline{SSH}(\tau_{classic})$. **Panel c**: long term sea surface temperature, in $°C$, for CTRL experiment. The **Panel d** is the long term difference of SST (in $°C$), i.e. $\overline{SST}(\tau_{ocean}) - \overline{SST}(\tau_{classic})$.

## 4.3 Extreme events study

In this section we focus on shorter time and space scales. We specifically try to characterize the extreme events that we may catch with such reduced sampling. We seek two goals with such approach. First we have seen in the previous chapter 3 that some positive events ($\tau_{ocean} > \tau_{classic}$) occur in the Southern Westerlies area with low probabilities of occurrence, in contrast with the mean negative effect and therefore want to characterize them. Secondly, since we do not have measures at the synoptic scale to be compared to, we rather search for evidences of the physical mechanisms at play, providing in that way some sort of conceptual validation. One of the phys-

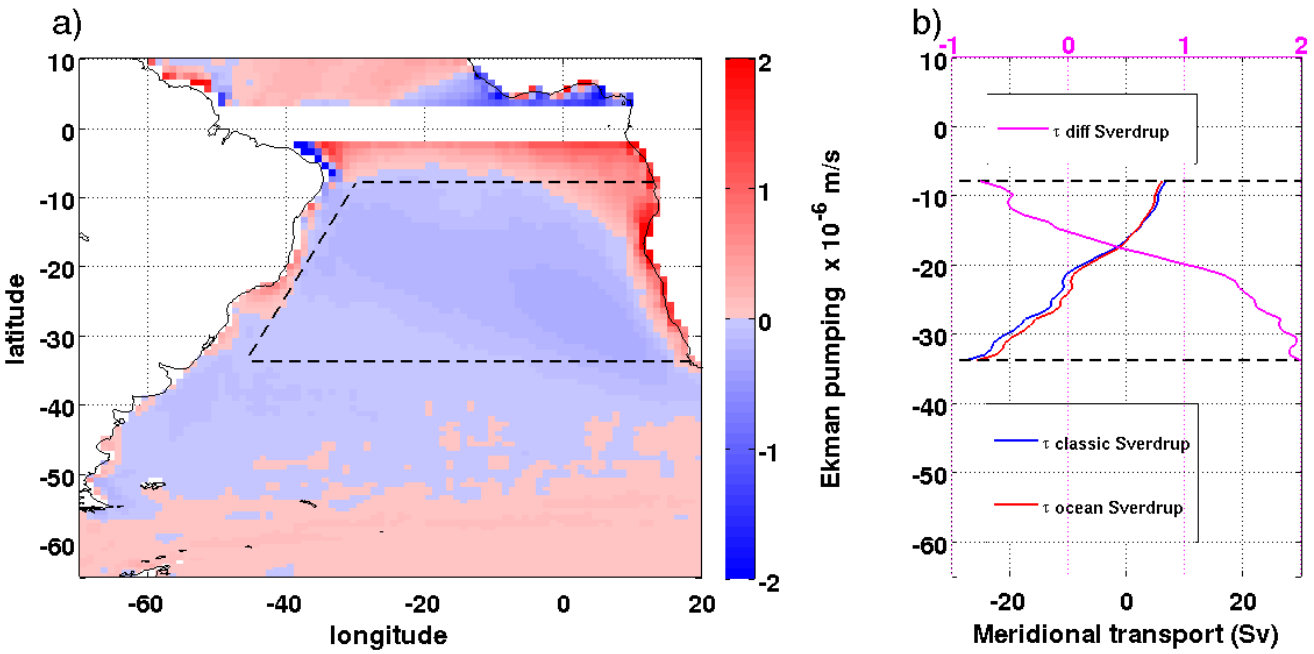


Figure 4.4: **Panel a**: Mean Ekman pumping difference in m/s for the period 2001-2010, i.e. $(\nabla_h \times \vec{\tau}_{ocean} - \nabla_h \times \vec{\tau}_{classic})/(f\rho_0)$. The over bar symbol (for time average) has been omitted for clarity. The black doted lines represent the integration area for the Sverdrup meridional transport. **Panel b**: Mean Sverdrup meridional transport in Sv for the period 2001-2010 for the classic stress (blue) and the wave-modified case (red). The meridional stream function of the depth integrated meridional Sverdrup transport is calculated as follow: $\int(\nabla_h \times \vec{\tau})/(\beta\rho_0)dx$, with $\beta = df/dy$. The second horizontal axis (magenta) is used for the transport difference (Sv) between the wave-modified and the classic approaches.

ical mechanisms responsible for the second effect (momentum fluxes modification, equation 2.7) is the wave breaking, which occurs more frequently for energetic events and is triggered only from a certain threshold (see BABANIN [1]). We try to correlate those small scale effects to physical mechanisms searching for metrics able to give statistical meaning (over a decade). To do so we build a Hovmöller diagram to study positive events of the Southern Westerlies area. We choose to explore the zonal variations of relative stress difference $(\tau_{ocean} - \tau_{classic})/\tau_{classic}$, i.e. along the propagation direction of the dominant winds. A space average is done along the meridional direction (the area is the one shown in figure 3.1 and defined in introduction). This allows us to "catch" a greater number of meteorological events and thus increase the statistical confidence. We zoom in on a three month period, from August to October 2006 (see figure 4.5), with intense storm events (maximum from 2001-2010 period) to be able to better distinguish the *space* × *time* variability on the diagram. The 10-year period exhibits a general behaviour very similar to the period retained for exemplification.

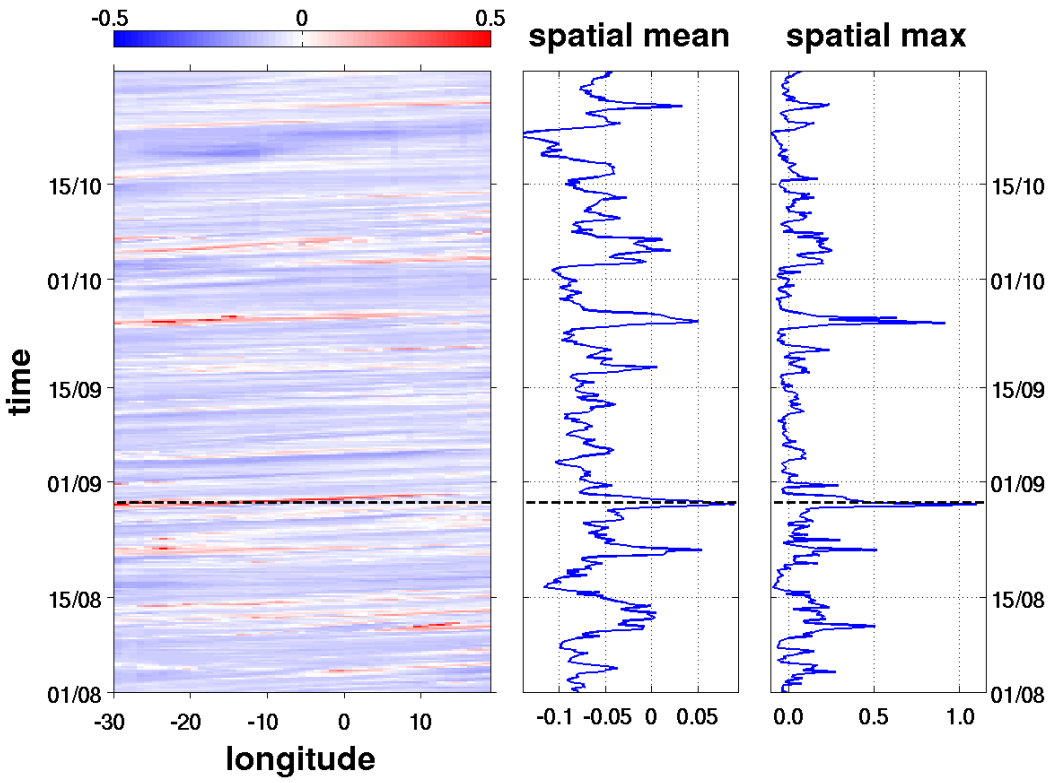


Figure 4.5: **Left panel**: Hovmöller diagram for the relative stress difference, i.e. $(\tau_{ocean} - \tau_{classic})/\tau_{classic}$ for August to October 2006 between longitudes 30°W and 20°E. A meridional space average is done between latitudes 55.5°S and 44.6°S. **Middle panel**: Zonally-averaged relative stress difference. **Right panel**: Maximum relative stress difference along the zonal width (30°W to 20°E). The doted line on each panel marks the first event illustrated in the section 4.4.

The mean and maximum values given in the central and right panels of figure 4.5 are computed along a distance close to 3500 km (the width of the Southern Westerlies area shown in figure 3.1). Nevertheless, the propagating pattern exhibited on the left panel clearly shows that this averaging is able to provide information on synoptic events at the time scale of a few days, allowing us to characterize the most intense storms.

We see that the difference is negative in the mean (central panel), consistent with the results of the chapter 3, with local departures of stress difference up to 110% of the classic value (right panel). The corresponding absolute value for this maxima is 0.486 $N/m^2$, creating a surface current difference (between WAVE and CTRL experiments) of 0.215 m/s (88.7% of the CTRL run surface current value). The scatter plot of the model response (surface current difference) is plotted against the stress difference for the full period in figure 4.6 for the Southern Westerlies area. A strong correlation (0.902) is found between the two axis.

This approach has been conducted for the two other areas but with poor results

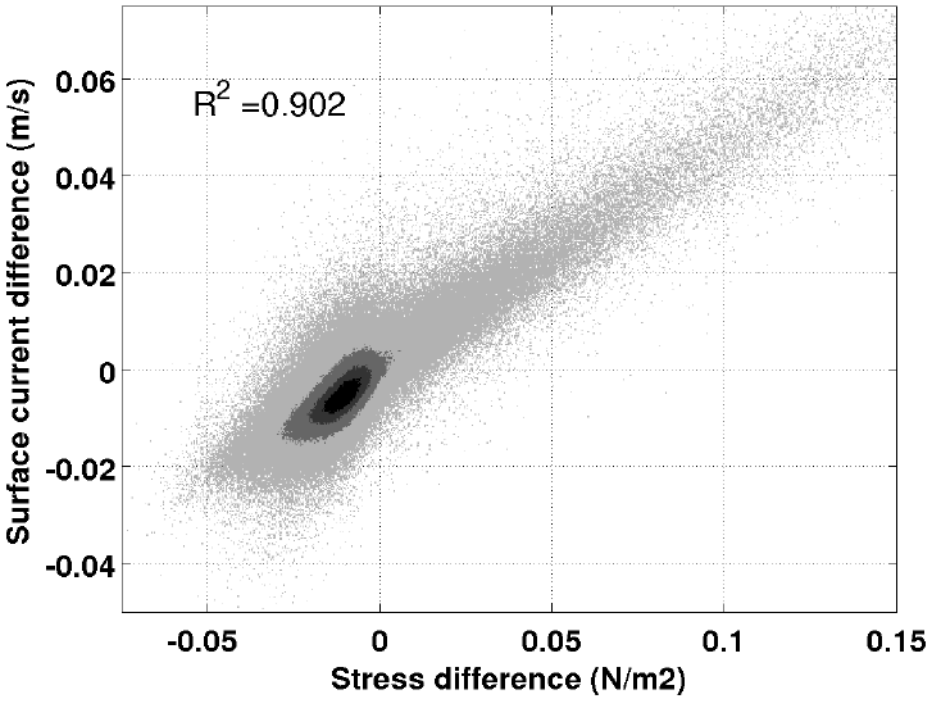


Figure 4.6: Scatter plot of surface current difference, i.e. $U_{surf}(\tau_{ocean}) - U_{surf}(\tau_{classic})$ (in m/s) versus the stress difference, i.e. $\tau_{ocean} - \tau_{classic}$ (in $N/m^2$) for the Southern Westerlies area for the 2001-2010 period. Data from the Hovmöller diagrams of current and stress differences are used. The linear correlation coefficient between the two sets of data is given ($R^2$).

for the stress/surface current correlation. The main reasons suggested to explain this are: Very few to no positive events occur for those areas (see figure 3.2 lowest two panels) which are not offshore storm tracks as the Southern Westerlies area is. Moreover the model surface current response seems to be corrupted with some numerical instability in the Trade winds area for periods close to one day (evidenced in spectral analysis, not shown). The SE Brazil area in its turn is subjected to many effects including the intense Western Boundary Current intensification. We have seen that although the model has a coarse resolution reputed not precise enough to catch such feature, it is actually modelled and have an influence in the ocean upper region not directly dependant on the local wind forcing.

Focusing on Southern Westerlies area, correlations of surface current difference with wave-related parameters have been sought to link the positive events exhibited in the Hövmoller diagram. The following parameters were explored: integrated wave parameters (Hs, Tp, wave slope), wave ages (full spectrum, swell and wind waves) and opposition index of propagating directions of: total waves, swell, wind waves and wind. [2] No clear correlation has been identified although the strongest positive

[2] The opposition index of two propagating directions equals 1 when the two directions difference

events ($U_{surf}(\tau_{ocean}) - U_{surf}(\tau_{classic})$) seem linked to steep waves, older wave age and opposition between waves and wind.

We have identified strong positive events and a high correlation between their mean effect (meridional average) and the propagation of storms. In the absence of reliable statistical results correlating the positive events to some physical parameters, we focus on even smaller time scale of single events (storms).

## 4.4 Single event illustration

Two intense events (low pressure cyclones) producing positive difference of surface current are presented in this section: the first one is the one highlighted in figure 4.5 of section 4.3 (black doted line, end of August 2006) and is of academic interest. A low pressure cyclone with its centre located near 23E/55S generats strong winds (figures 4.7 and 4.8, panel a) "wind"). A second event of more practical impact, i.e. closer to the Brazilian coast, is found during September 2006 near the Southern coast of Brazil and is shown in figures 4.9 and 4.10. Once again it is associated with strong winds. The events are presented at their climax were the current difference reaches its maximum. This also corresponds to the maximum of wind speed and of positive stress difference. The surface current difference (shown in panels e) of figures 4.7 and 4.9), i.e. $U_{surf}(\tau_{ocean}) - U_{surf}(\tau_{classic})$ reaches 0.56 m/s (0.31 m/s) for the first (second) event which represents 43% (24%) of the classic forcing current (CTRL experiment).

Both wave effects are illustrated together with the total effect in a first figure for each effect (figures 4.7 and 4.9). The spacial anti-correlated behaviour between the two effects is visually evident (comparing panel b) "$1^{st}$ effect" versus panel c) "$2^{nd}$ effect"), as well as the higher relative importance of the first effect over the second one, consistent with the results of the Chapter 3. The same wave-related parameters listed at the end of the last section 4.3 are explored in an attempt to correlate the two wave effects with physical parameters. The results are shown in a second set of figures where each effect is plotted against its most correlated wave-related physical parameter (figures 4.8 and 4.10). The first effect is found to correlate well with the mean square slope of the wave (integrated parameter available from ERA-20C reanalysis), as can be seen comparing panels b) "$1^{st}$ effect" and c) "Wave slope". This is highly consistent with the parametrization of this first effect based on the absorption ratio of momentum flux by waves (see Appendix B.3). Indeed a young, developing sea state, is related to steep waves. The second effect best correlates with a higher wave age of the wave full spectrum, as can be seen comparing panels d "$2^{nd}$

is 180°, zero for a relative angle of 90°and equals -1 when both elements propagate in the same direction.

effect" and e) "Wave age" of figures 4.8 and 4.10. This is also consistent with its parametrization based on the difference between wave dissipation and absorption of momentum fluxes (see equation 2.7). Older waves (wave age greater than 1.2) are the most likely to have such momentum flux difference positive towards the ocean.

The linear correlation coefficient (along time) between the main parameters involved in this section are computed for the full domain and the Southern Westerlies area (over the year 2006) and the results are presented in table 4.3. The correlation coefficients related to the two extreme events studied have been explored over the lifespan of each event with a space domain centred on, and moving along the storm track (squared region about $30° \times 30°$, not shown). The results are found very sensitive to the time duration and the type of difference considered (ratio or difference) and are therefore not presented. It is worth mentioning though that the general behaviour is similar with the Southern Westerlies area one, with anti-correlated wave effects and reasonable correlations of wave slope and wave age with first and second effects respectively. One robust result of this event-restricted correlation study is the spacial anti-correlation at each time step between the two effects. Those coefficients are high, consistent with the visual inspection previously mentioned between panels b) "$1^{st}$ effect" and panel c) "$2^{nd}$ effect". The correlation is -0.72 (-0.53) for the difference $\tau_{ocean} - \tau_{classic}$ (ratio $\tau_{ocean}/\tau_{classic}$) for the first event at the time shown on figure 4.7, and -0.88 (-0.68) for the second event of figure 4.9.

| $R^2$ | Total effect | | *1st effect* | | *2nd effect* | | **MSqSlope** | | **Wave age** | |
|---|---|---|---|---|---|---|---|---|---|---|
| Wind | 0.73 | 0.44 | **0.78** | **0.79** | -0.40 | -0.44 | 0.84 | 0.93 | -0.71 | -0.76 |
| Total effect | | | 0.80 | 0.61 | 0.17 | 0.41 | 0.77 | 058 | -0.63 | -0.24 |
| *1st effect* | | | | | -0.45 | -0.47 | **0.57** | **0.77** | **-0.84** | **-0.73** |
| *2nd effect* | | | | | | | -0.25 | -0.29 | **0.46** | **0.60** |
| MSqSlope | | | | | | | | | -0.42 | -0.60 |

Table 4.3: Linear correlation coefficients between the following variables: Wind (10-m neutral wind), total wave effect ($\tau_{ocean}/\tau_{classic}$), 1st wave effect ($\tau_a/\tau_{classic}$), 2nd wave effect ($\tau_{ocean}/\tau_a$), wave mean square slope (MSqSlope) and total wave age (see figure 4.8 for the last two variables definition). Coefficients are given for the full domain (left) and Southern Westerlies area (right), for the 2006 year, in sub-cells for each variable combination.

Back to table 4.3 and the along-time correlations, we see that the wave age correlates well for both effects, and even better for the first effect, something that could not be seen on the panel e) "Wave age" of figures 4.8 and 4.10 due to the colour scale upper limit set to best catch the correlation with the second effect. The wave slope correlates well with the first effect for the Southern Westerlies area. It is to be noted that the wind intensity is a better (at least similar) correlation than the wave slope for the first effect and that it gives similar correlation than the wave

age for the second effect. This result is treated in the discussion chapter.

We notice in studying the specific events that the $2^{nd}$ effect has a greater spacial extent for positive difference than the $1^{st}$ one. For instance, in figure 4.7, the $2^{nd}$ effect is seen positive (red coloured) till a longitude of about 10E (panel c) while the $1^{st}$ effect spans only till the longitude 1W (panel b). This is consistent with the wave group velocity $c_g$ shown on figure 2.1, which has propagated in our cases in the general direction of the storm path. It is though hard to quantify the range of influence of the second effect since the wave origin is not easily traceable, even if we know that swell can propagate up to the coast line over thousands of kilometres.

We have identified at the scale of two particular events the wave effects on surface stress with large associated surface current differences. The main physical mechanisms have been graphically exposed and quantified with linear correlation coefficients.

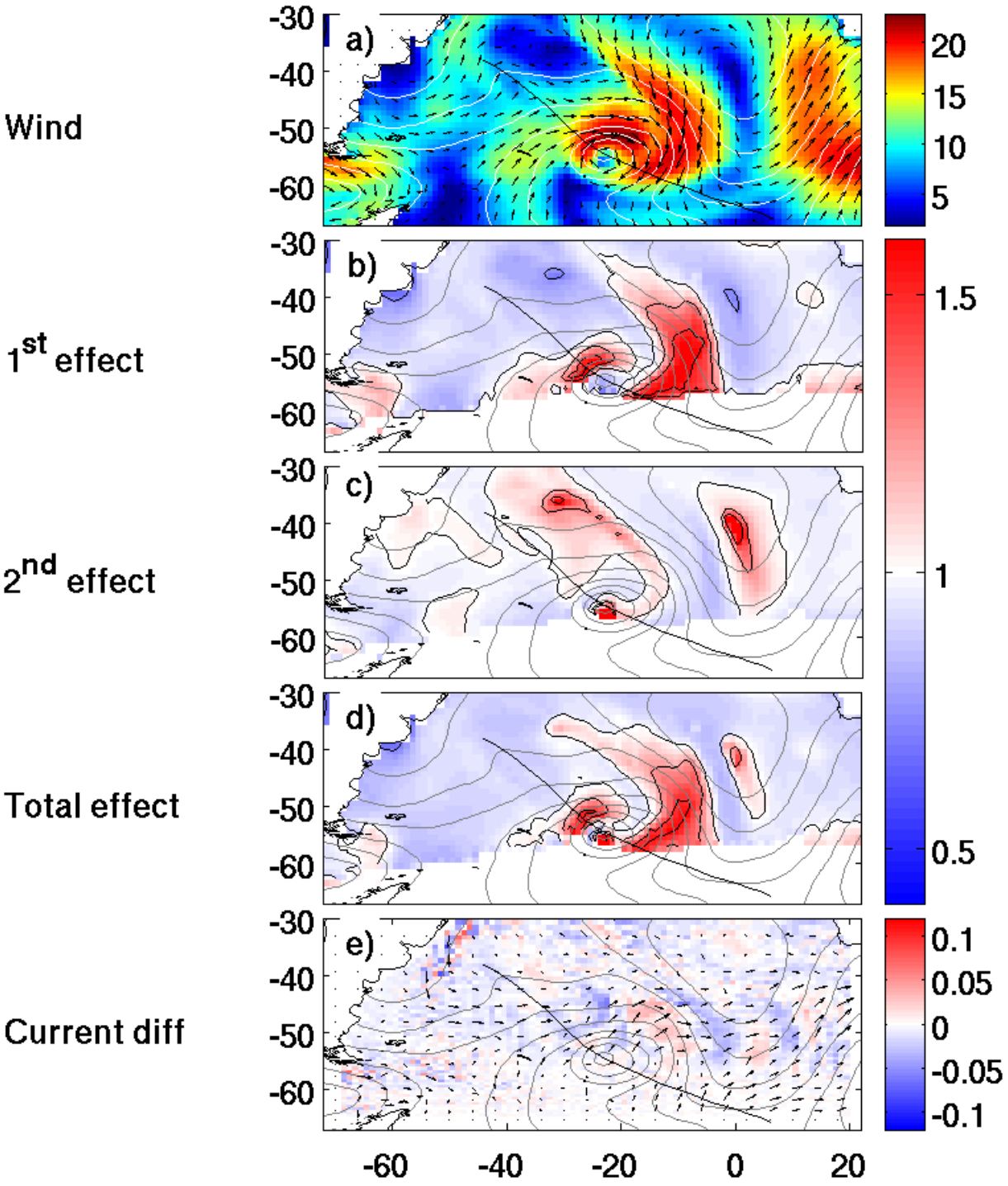


Figure 4.7: First positive event (i.e. $\tau_{ocean} > \tau_{classic}$) illustrated during a storm (low pressure cyclone) on 2006/08/29 at 03h UTC. Panel a) shows the 10-m wind (colour scale is wind speed in m/s and arrows wind direction). Panel b) to d) show respectively (colour scale + contour): the first effect ratio (i.e. $\tau_a/\tau_{classic}$), the second effect (i.e. $\tau_{ocean}/\tau_a$) and the total effect of waves (i.e. $\tau_{ocean}/\tau_{classic}$). The last panel e) is the surface current difference $U_{surf}(\tau_{ocean}) - U_{surf}(\tau_{classic})$ in m/s (colour scale) and the classic surface current (arrows). The mean sea level pressure (grey contour every 10 hPa) and the storm track (black line, moving Souteastward) during its active life (from 2006/08/27 09h UTC to 2006/08/31 03h UTC) are shown on each panel. The low pressure minimum is 947 hPa (first contour around is 950 hPa).

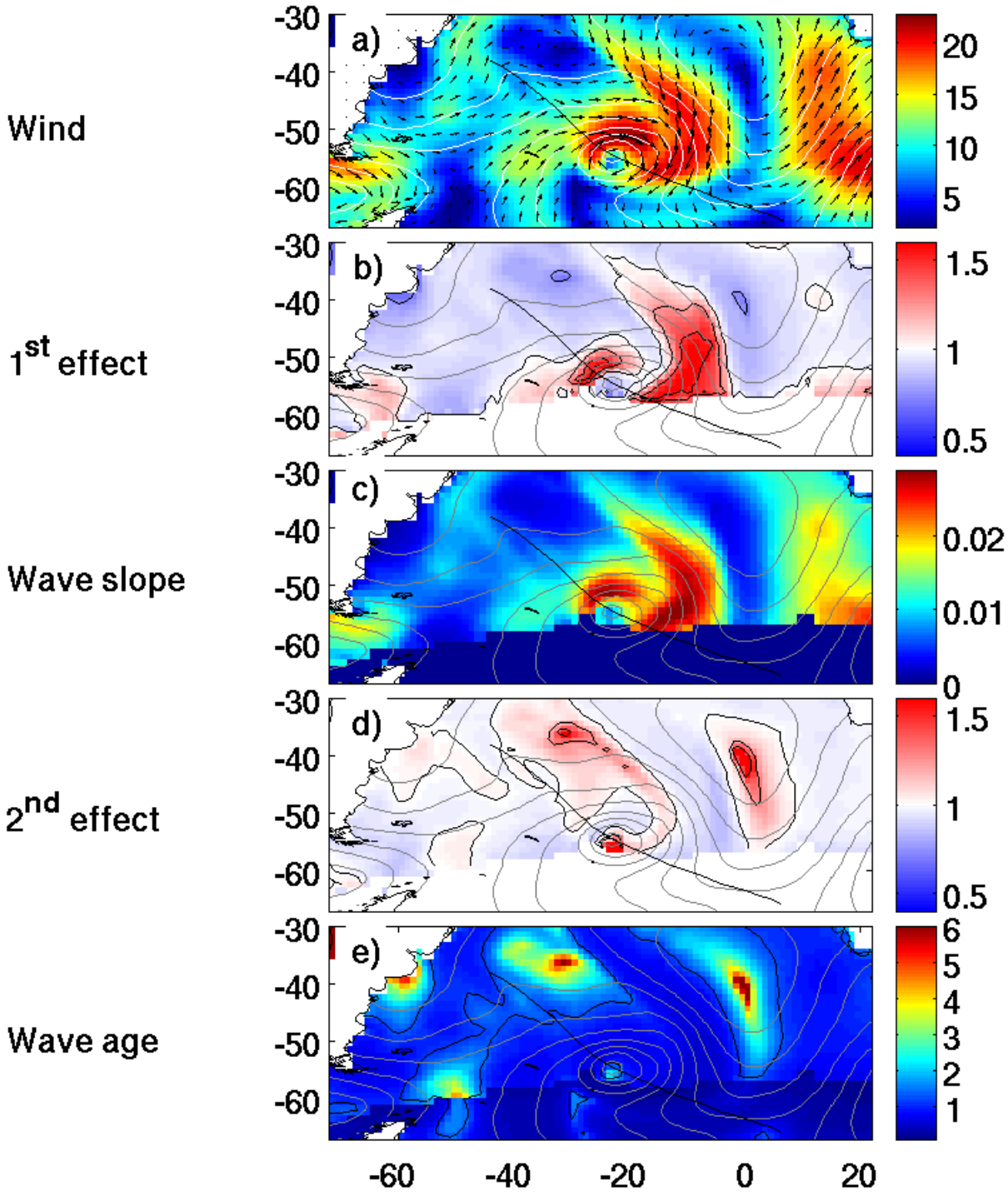


Figure 4.8: First event illustration on 2006/08/29 at 03h UTC: correlation of each wave effect with a physical parameter. Panels a), b) and d) are identical to panels a), b) and c) of figure 4.7 (wind, first and second wave effects). Panel c) is the mean square slope of waves (dimensionless) as downloaded on ERA-20C website and defined as: $\int\int k^2 F(f,\theta) df d\theta$, with $F$ the (full) energy spectrum, $f$ the wave frequency, $\theta$ the wave direction and $k$ the wave number as given by the linear dispersion relation. Panel e) is the wave age parameter, i.e. $c_p/U_{10}^n$ (colour shading), and the 1.2 limit between young and old waves (see EDSON *et al.* [18]) is denoted by a black line. The mean sea level pressure and the storm are shown on each panel as described in figure 4.7 legend.

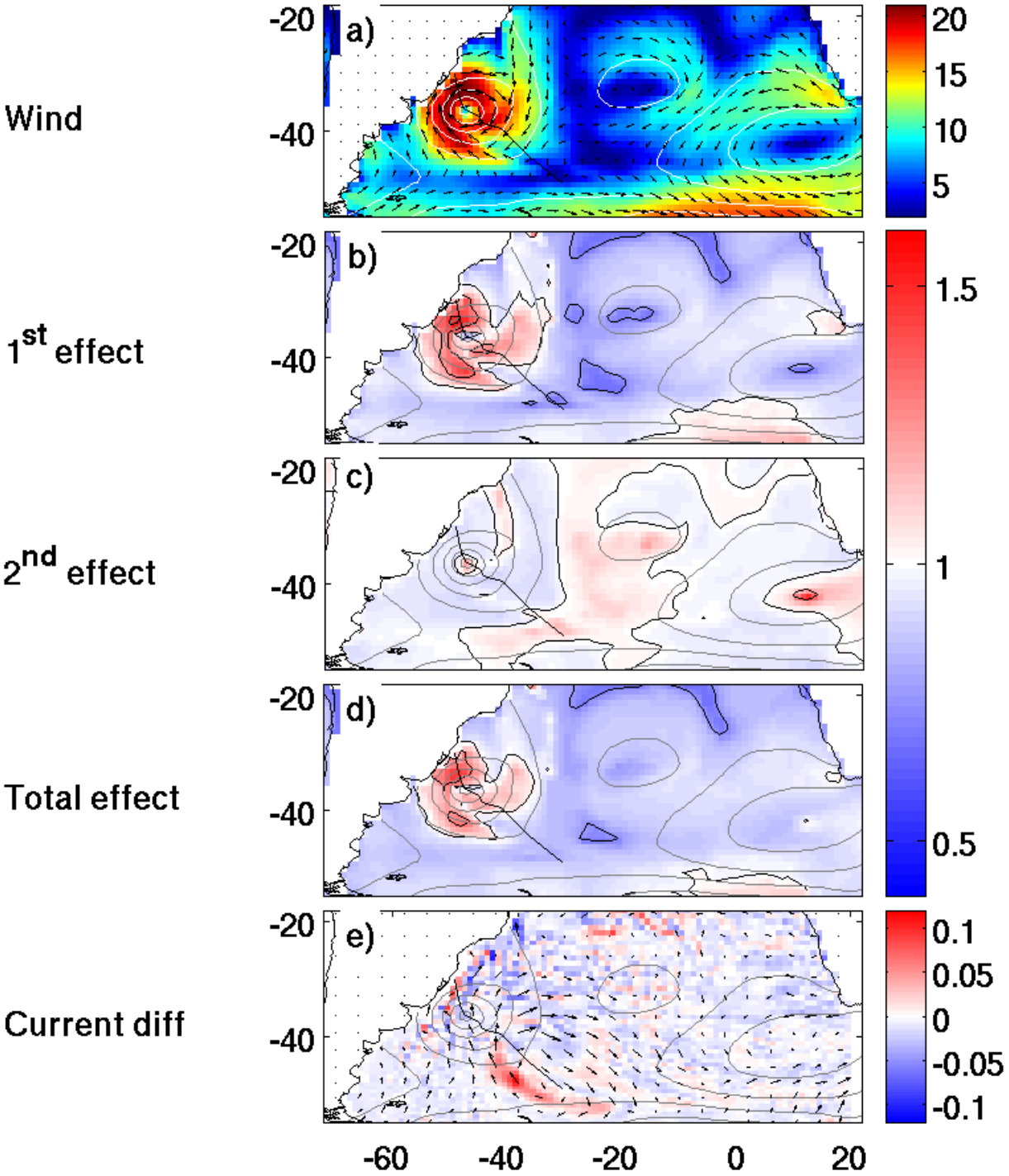


Figure 4.9: Second positive event (i.e. $\tau_{ocean} > \tau_{classic}$) illustrated during a storm (low pressure cyclone) on 2006/09/03 at 03h UTC. The storm is active from 2006/09/02 09h UTC to 2006/09/04 21h UTC (black line) moving South-Eastward. The low pressure minimum is 968 hPa (first contour around is 970 hPa). See figure 4.7 for complementary legend.

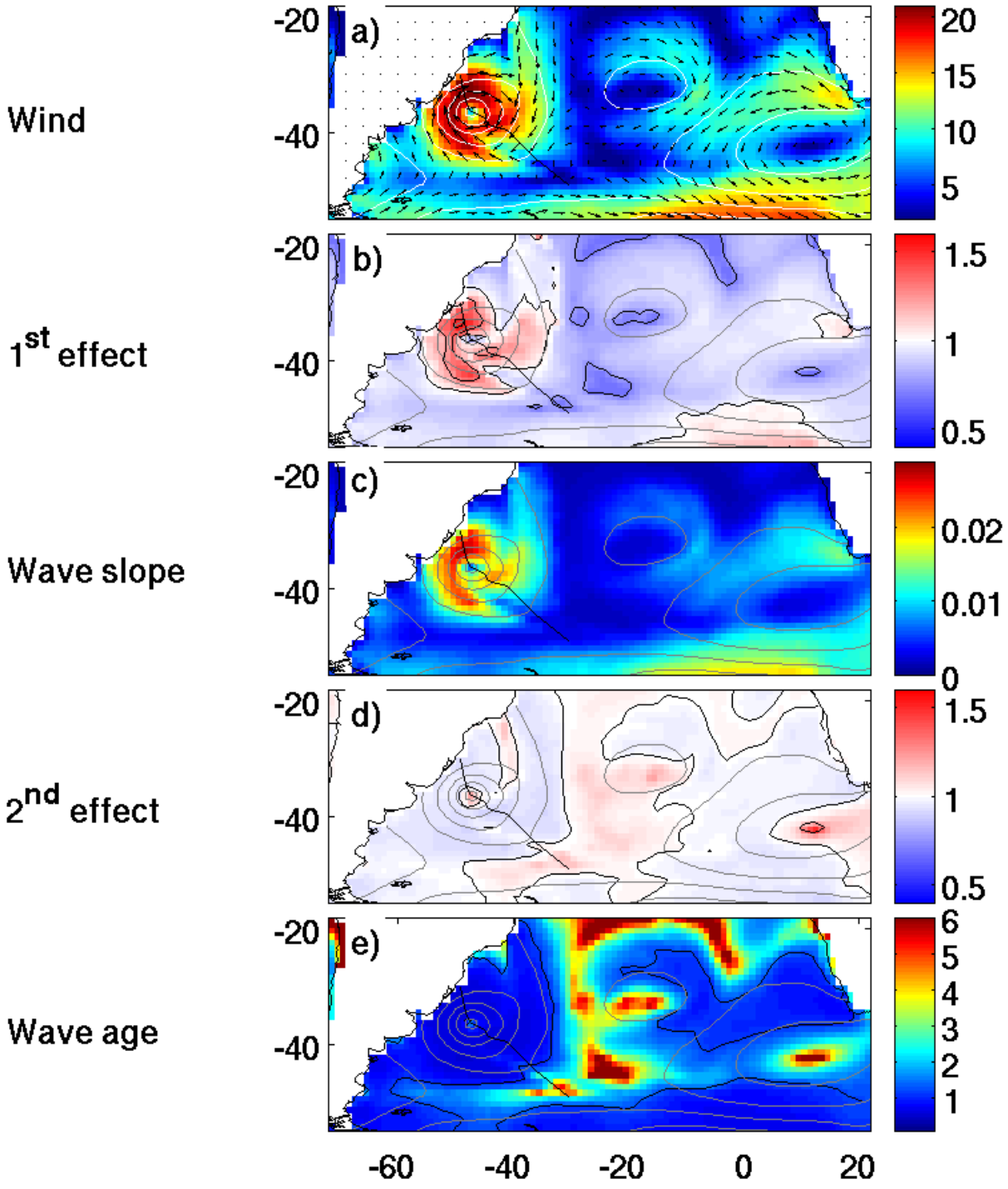


Figure 4.10: Second event illustration on 2006/09/03 at 03h UTC: correlation of each wave effect with a physical parameter. See figures 4.7, 4.8 and 4.9 for legend.

# Chapter 5

# Discussion

**Long term results** We have introduced a wave effect parametrization for the surface stress following BREIVIK *et al.* [10]. The Sea Surface Temperature differences shown in figure 4.3 are in good accordance with BREIVIK *et al.* [10] results (figure 1), with two common singularities in the Benguela upwelling area (positive difference) and near the Brazil-Malvinas confluence zone (negative difference). Our simulations probably exaggerate the wave effects, reaching up to 1°C difference while BREIVIK *et al.* [10] have a maximum closer to 0.5°C. This could be imputed to many differences in modelling set-up, a longer integration period and also to the different forcing sets. BREIVIK *et al.* [10] used ECMWF ERA-Interim forcing, which assimilates more data and is reputed more precise. We also used a different classic stress formulation: we used the formulation presented in appendix B.4 based on the modified Charnock equation while BREIVIK *et al.* [10] used a drag coefficient depending only on the neutral wind.

We compare our 10-year mean SST results to the WOA2009 climatology. The results are shown in figure 5.1 and the error variation is presented in figure 5.2. Except for extreme values (minimum and maximum), the spacial mean and standard deviation of the variation brought by the wave effect is one order of magnitude lower than the original bias. The whole domain sees almost no impact on SST with a slightly hotter (than it already was) SST mean value, but with a spacial variability a little closer to the reference (0.5% difference on Root Mean Square Difference, see table 5.1). The CTRL run clearly performs better than the WAVE run for the Benguela upwelling. This local result tendency is not provided by BREIVIK *et al.* [10] and we do not know whether it comes from the HYCOM model low resolution or from a tendency brought by the wave effect. The Brazil-Malvinas mean SST, in its turn, is globally closer to WOA2009 under the wave effect (almost 4% of difference on RMSD towards the climatology, see table 5.1) but with some mixed results (both positive and negative error variation, see figure 5.2) probably due to a different geographic location between the original bias and the difference brought

by the wave effects. Detailed maps of those two regions can be found in appendix D as well as a bias comparison in boxplot format.

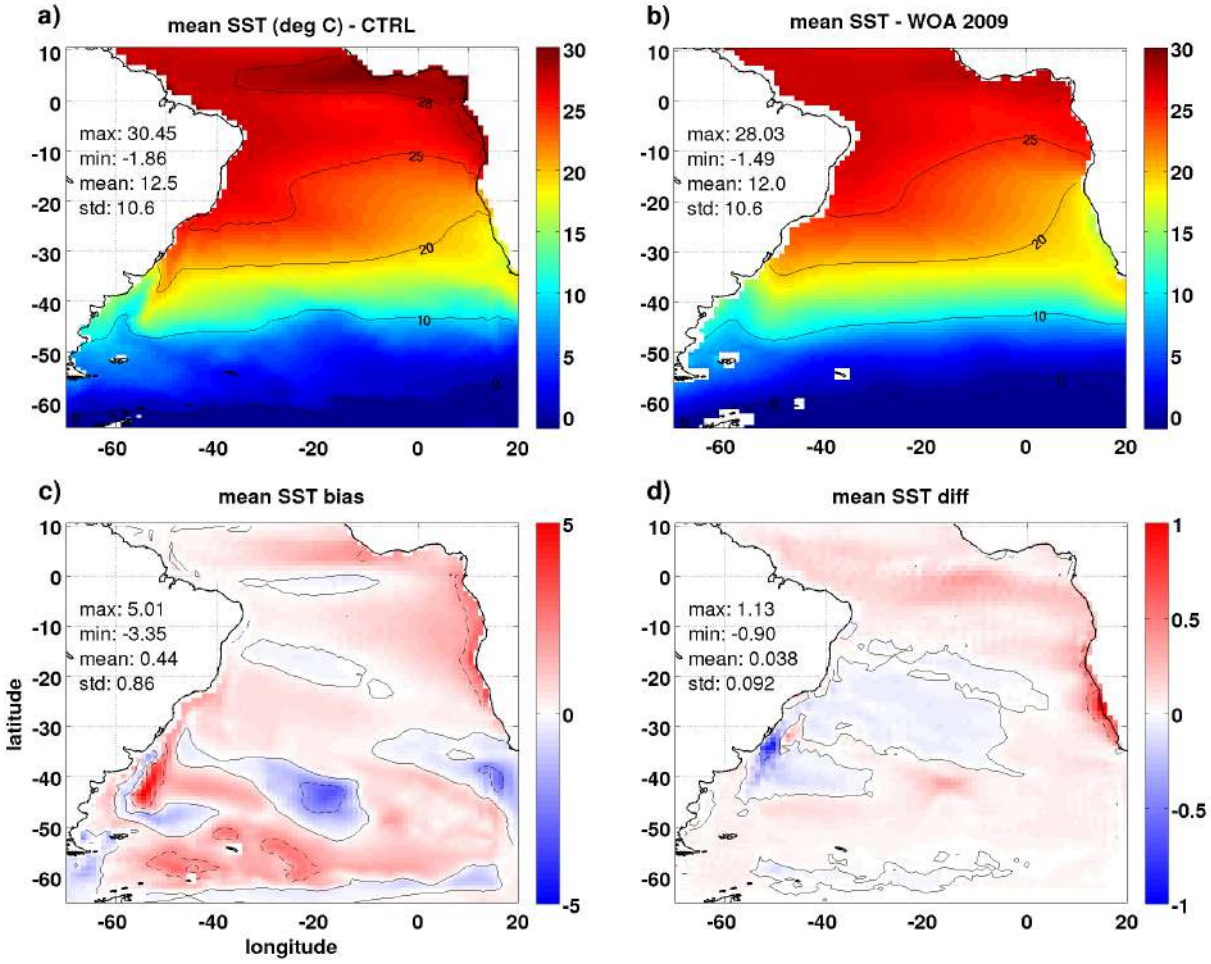


Figure 5.1: Long-term Sea Surface Temperature comparison. **Panel a**: SST long-term results for CTRL experiment **Panel b**: WOA2009 climatology results. **Panel c**: SST bias of classic approach (CTRL - WOA09). **Panel d**: SST difference (WAVE - CTRL). The doted/mixed lines for bias (difference) are the +2/-2 (+0.5/-0.5) contours.

The panel b) of the figure 5.2 is the the relative error variation (definition given in legend). A variation of $-100\%$ means that the difference from the wave effect completely compensates the original error (absolute value of the original bias) of the classic forcing approach (CTRL run). A value lower than that over compensates this error and anything above zero accentuates the original error. In practise, the wave effects seem to mainly accentuate the original bias with local improvements but never over compensating the original bias (minimum value found is 99.9%).

A similar approach is conducted with the mean Sea Surface Height from HYCOM results which are compared to the Mean Dynamic Topography (MDT), i.e. the mean

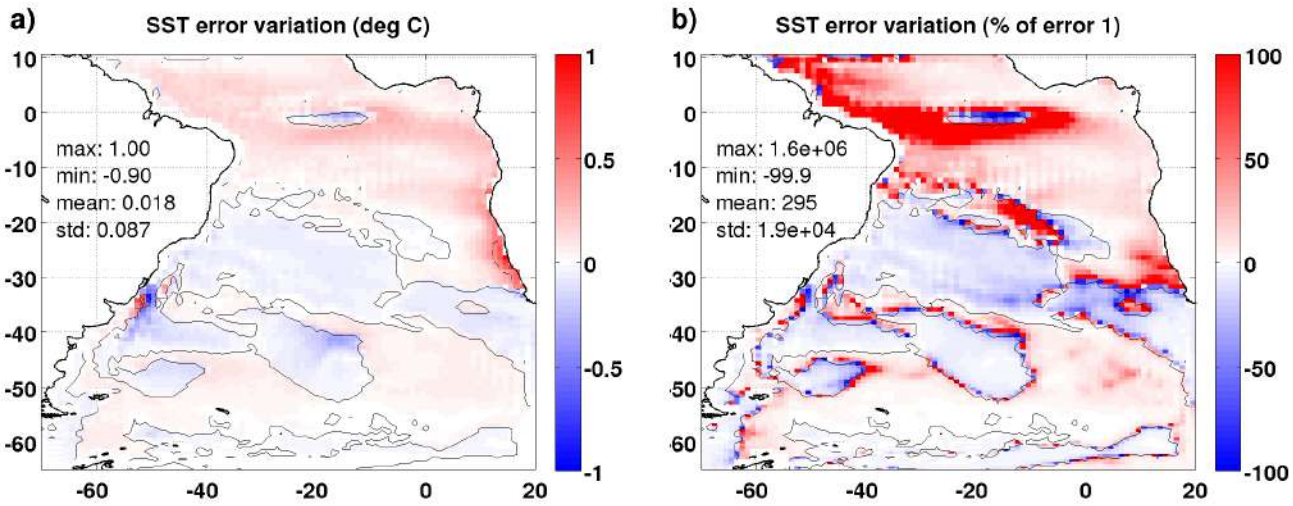


Figure 5.2: Sea Surface Temperature error variation. **Panel a**: Absolute error variation, i.e. | WAVE - WOA09 | - |CLRL - WOA09|. **Panel b**: Relative error variation, i.e. | WAVE - WOA09 | - |CLRL - WOA09| / |CLRL - WOA09|.

sea surface height above geoid, MDT_CNES-CLS13. [1] The spacial statistical values (minimum, maximum and standard deviation) of the wave difference are one order of magnitude lower than the original bias of the classic approach. The spacial mean value is one order of magnitude greater but is not of great significance since it is the SSH spatial variability which leads the barotropic/geostrophic circulation. The figure equivalent to the SST figure 5.1 is shown in appendix figure D.6.

Finally it is hard to conclude on the benefits/damages brought by the wave effects since the HYCOM model is not originally set-up to give precise results due to its low resolution and the many simplifications used.

**Single events** At the event scale, ZHANG *et al.* [7] found a maximum surface current difference of 0.4 m/s for an associated (to the event) maximum wind speed slightly below 14 m/s and stress difference of up to 0.3 $N/m^2$. Our events of the section 4.3 are more intense and therefore hard to use for comparison. In a attempt to compare our results, we build a scatter plot of surface current difference versus wind speed of our Southern Westerlies area for the year 2006 (figure D.7 in appendix). We find a maximum surface current difference of 0.24 m/s for the 13-15 m/s wind speed range. It is to be noted that only the first wave effect is implemented in ZHANG *et al.* [7] work, giving a probably too vigorous wave effect (no anti-correlated second effect weakening the total effect) and a first reason for the difference between the two results. Another possible explanation of the difference lies in the horizontal

[1] MDT_CNES-CLS13 was produced by CLS Space Oceanography Division and distributed by Aviso, with support from Cnes (http://www.aviso.altimetry.fr/) [accessed 2016/11/22].

| SST statistics | models | Mean | RMSD | SDT |
|---|---|---|---|---|
| Full domain | WOA09 (ref.) | 11.99 | 0 | 10.55 |
| | CTRL | 12.44 | 0.862 | 10.55 |
| | WAVE | 12.47 | 0.858 | 10.57 |
| Benguela upwelling | WOA09 (ref.) | 18.87 | 0 | 2.30 |
| | CTRL | 19.09 | 0.76 | 2.58 |
| | WAVE | 19.17 | 0.82 | 2.57 |
| Brazil-Malvinas confluence | WOA09 (ref.) | 14.62 | 0 | 5.17 |
| | CTRL | 15.28 | 1.10 | 5.45 |
| | WAVE | 15.26 | 1.06 | 5.39 |

Table 5.1: SST difference long-term statistics for 3 areas and for the two runs plus the WOA2009 climatology. The Mean values, the centred Root Mean Square Difference (with the reference taken as WOA09) and the Standard Deviation are given (in degree Celsius). RMSD and STD are made on the geographical domain and thus characterize the spatial variation of the mean SST.

resolution (1/6°) used by ZHANG *et al.* [7], allowing to catch finer current variation due to the increased gradient resolution. Considering the full wind speed range of our results, the maximum surface current difference found is 0.56 m/s. The scatter plot and the distribution shown in appendix also reveal that our extreme events are sensitive to the wind range selection. Indeed, some stronger current difference happens for smaller wind range (around 12 m/s), something counter intuitive. A longer period than one year would be necessary to study, together with a proper statistical analysis of the extremes.

**Wave age dependency** A reasonable dependency to wave age is found with momentum flux transfer (both effects, see table 4.3). The wind has a similar correlation coefficient with the first effect than the wave age and wave slope. This is consistent with EDSON *et al.* [18], who states that wave-age and wave-slope dependences do not bring much to momentum flux parametrizations when compared to wind-dependant parametrizations. "Momentum flux parametrization" in this case is to be understood as the first effect, since the drag coefficient and the lower atmosphere shear are treated in EDSON *et al.* [18] work. The main reason given there is that there is a quasi linear relationship between inverse wave age and the 10-meter wind. The wave information is, on the other hand, of greater importance for the parametrization of the second effect of our work, as can be seen in the highest correlation coefficient, among all combinations, between wave-age and the second effect (table 4.3).

# Chapter 6

# Conclusion

A wave-dependent parametrization of the surface stress has been introduced. The total wave effect is divided into two sub effects. The first one is linked to the modification of the drag coefficient by the wave field, for instance young developing waves being prone to create a rougher surface. The parametrization of the Charnock coefficient, the parameter driving the wave-modified drag coefficient, is based on two stress results available from third generation wave models such as WAM. Those two stresses are the air-side stress and the stress absorbed by the wave field while developing. The second effect takes into account all stress results provided by the wave model to make the net sum of stress going to the ocean: the absorbed (by the wave field) stress fraction is subtracted from the air-side stress and the dissipation stress is added, giving the net stress going to the ocean. The total wave effect is the combination of both effects presented above.

Based on the available results of the coupled wave-atmosphere ERA-20C reanalysis, we have first characterized the stress variations under wave effects for the South Atlantic. We have evidenced a global mean effect reducing the surface stress, a negative difference of -7% of the classic mean stress value for the entire domain (see figure 3.1). Local positive events of stress difference are mainly happening during storm events in the Southern part of our domain (figure 3.2), with positive stress difference of up to 59% of the classic stress. The two sub effects are found anti-correlated one with the other. The first effect (wave-modified drag coefficient) is the one mainly responsible for the total effect, as shown by its higher linear correlation with the total effect (0.78 for the entire domain) compared to the correlation of the second effect (0.19).

The impact of this stress variation has been studied through the comparison of two numerical experiments of the HYCOM ocean circulation model over a decade. Consistently with the initial input data analysis, the mean wave effect is a reduction of the South Atlantic gyre intensity, with a Sverdrup transport variation of 1 to 2 Sv (see figure 4.4). Two local signatures of this effect in SST variation (long term

results) have been found consistent with BREIVIK *et al.* [10] even though sightly stronger in our case (figure 4.3). The Benguela upwelling area is up to 1.1 °C hotter under wave influence and the Brazil-Malvinas confluence is up to 0.9 °C colder. The long term comparison of the mean SST with WOA2009 climatology shows a small reduction of the bias in the Brazil-Malvinas region and an increase of this bias for the Benguela upwelling area and the entire domain. Those results are to be taken with great caution (see chapter 5). Indeed the model is not configured to provide realistic results but rather to make a robust basis for comparison. In that sense the model performs well and the results are consistent with the expected variations due to the modification of the forcing fields.

The local departure of positive events has been characterized and found correlated to storm events (section 4.3), producing large surface current differences of up to 0.56m/s which is 43% of the current speed under classic forcing (figure 4.6). We have shown that the first effect has a strong correlation with the wave slope (and the inverse wave age) but remains best correlated to the wind itself (section 4.4). The second effect in its turn is best correlated to the wave age.

**Perspective and future works**

We have seen that the actual model set-up gives a solid basis for comparison, but is not originally designed to provide realistic results. Dis-considering this fact for the sake of discussion and to provide axis of future work, if the model was to be used for realistic results, two criticisms could be produced to the scheme presented here.

The first one is link to the fact that "only" one wave effect is used (stress modification) while waves are known to influence many other physical parameters. Having a large difference is somewhat an expected result then. Indeed we bring a parametrization among a set of "well balanced" parametrizations all tuned together to best fit observations. The second point is that the two effects (drag coefficient and flux distribution) are themselves based on other parametrizations of the wave model (e.g. growing and dissipation rates) which are in the first place tuned to give good results mainly for significant wave height and wave period. Thus we heavily rely on results not tailored to achieve good performance for the desired parameters, which are in our case the total stress going to the ocean.

Having said that, the fact of coupling and including the wave model results seems undoubtedly the right path in the sense that more physics is included and it thus brings a better understanding of the atmosphere-waves-ocean system dynamic and more possibilities to finely tune the model. This process is beginning in the Physical Oceanography Lab - LOF/GRUPO and even if the first results do not seem to bring obvious bias or error reduction, they brought a robust basis for comparison and

understanding of the wave effects, showing that the effort toward models coupling needs to be continued and intensified.

In that sense, further investigations on the two following points are necessary:

- Include more wave effects to try to equilibrate the global set of parametrizations in a consistent manner. Those parametrizations are already available and documented (see BREIVIK *et al.* [10]). This could also imply to explore and compare other parametrizations of wave models (run a benchmark) than the used one (WAM)

- Perform our own wave-modified forcing fields and run the HYCOM model with finer resolution to further investigate the two singularities identified in this study (Benguela upwelling and the Brazil-Malvinas confluence) with a model set-up allowing realistic results.

As mentioned in 3.1, we used a forcing frequency of 6 hours. Actually data are available 3-hourly but the available computational capabilities dictated us to restrict ourselves to a lower frequency. A future work could make the best of the available high frequency data (3-hourly) together with a higher resolution grid (1/4 and 1/12° are used on a daily basis in our lab and in the REMO network [1] ) to improve the representation of the synoptic behaviour and highlight furthermore the wave-induced variability described in 4.4. One possibility for the long term analysis is to compare the time-varying SSH anomaly observations (weakly/monthly values) provided by AVISO with an eddy-permitting HYCOM model (1/4° resolution or finer) to evaluate the wave impact on the variability of mesoscale processes. Focusing on the numerical model evaluation, a study of the 3 dimensional structure of the wave influence could bring new insights, with emphasis on the two identified regions of hight variability: Benguela upwelling system and the Brazil-Malvinas confluence.

The KPP profile parametrization (LARGE *et al.* [27]) used in HYCOM is driven by the friction velocity $u_*$ and thus depends on the surface stress. In the actual configuration of the model, the KPP parametrization relies on a friction velocity internally calculated based on the wind speed. It is then an easy step to include the effect of the waves using instead the $\tau_{ocean}$ stress for friction velocity calculation and the KKP profile determination. As mentioned in the introduction, other effects influence the ocean upper-part, e.g. the turbulent mixing and the Stokes-Coriolis effect. BREIVIK *et al.* [10] run various models with new parametrizations that could be tested.

[1] http://www.rederemo.org/html/ [accessed 2016/12/06]

As mentioned in section 2.1, the wave field acts as a reservoir of momentum flux capable of transporting energy at the wave group velocity $c_g$ and giving it back elsewhere. This has been evidenced is the section 4.4 where positive stress difference is shown to occur away from the assumed production site (low pressure cyclone).

Further study could be done on the wave model results to try to identify and quantify the part of swell-transported energy lost to the ocean upper part before it reached the coast line. This might be the case in a number of situations such as wind wave propagating against wind, wave propagating against surface currents. This piece of information is of interest as it gives an estimate of potential impact on surface currents.

It is worth noting that some more physical effects are involved in energy transfer/loss which are not implemented in the version of the wave model that we have used. This is still an area under investigation with different physical mechanisms responsible for the air/sea fluxes suspected and explored. See for example ARDHUIN *et al.* [28] and the energy lost by the swell during its propagation due to air-sea (turbulent) interactions.

# Bibliography


[1] BABANIN, A. V. *Breaking and Dissipation of Ocean Surface Waves*. Cambridge, UK, Cambridge University Press, 2011. ISBN: 9781107001589.

[2] CRAIG, P. D., BANNER, M. L. "Modeling wave-enhanced turbulence in the ocean surface layer", *Journal of Physical Oceanography*, v. 24, pp. 2546–2559, 1994.

[3] MCWILLIAMS, J. C., RESTREPO, J. M. "The Wave-Driven Ocean Circulation", *Journal of Physical Oceanography*, v. 29, pp. 2523–2540, 1999.

[4] BABANIN, A. V., HAUS, B. K. "On the existence of water turbulence induced by nonbreaking surface waves", *Journal of Physical Oceanography*, v. 39, pp. 2675–2679, 2009.

[5] JANSSEN, P. A. E. M. "Wave-induced stress and the drag of air flow over sea waves", *Journal of Physical Oceanography*, v. 19, pp. 745–754, 1989.

[6] ECMWF. *IFS Documentation CY38r1, Part VII: ECMWF Wave Model*, 2013.

[7] ZHANG, H., SANNASIRAJ, S. A., CHAN, E. S. "Wind Wave Effects on Hydrodynamic Modeling of Ocean Circulation in the South China Sea", *The Open Civil Engineering Journal*, v. 3, pp. 48–61, 2009.

[8] DENG, Z., HAN, G., ZHANG, X., et al. "Impacts of surface wave-induced Coriolis-Stokes forcing on the upper ocean circulation", *Journal of Oceanography and Marine Science*, v. 2(4), pp. 102–121, 2011.

[9] BABANIN, A. V., GANOPOLSKI, A., PHILLIPS, W. R. C. "Wave-induced upper-ocean mixing in a climate model of intermediate complexity", *Ocean Modelling*, v. 29, pp. 189–197, 2009.

[10] BREIVIK, Ø., MOGENSEN, K., BIDLOT, J.-R., et al. "Surface wave effects in the NEMO ocean model: Forced and coupled experiments", *Journal of Geophysical Research: Oceans*, v. 120, pp. 2973–2992, 2015.

[11] BLECK, R., HALLIWELL, G., WALLCRAFT, A., et al. *HYbrid Coordinate Ocean Model (HYCOM)*, 2002.

[12] POLI, P., HERSBACH, H., TAN, D., et al. *The data assimilation system and initial performance evaluation of the ECMWF pilot reanalysis of the 20th-century assimilating surface observations only (ERA-20C)*. Relatório Técnico 14, Shinfield Park, Reading, UK, 2013. Disponível em: <http://www.ecmwf.int/publications>.

[13] STULL, R. B. *An Introduction to Boundary Layer Meteorology*. Kluwer academic publishers ed. Dordrecht, The Netherlands, 1988. ISBN: 9027727694.

[14] CHARNOCK, H. "Wind stress on a water surface", *Quarterly Journal of the Royal Meteorological Society*, v. 81, pp. 639–640, 1955.

[15] JANSSEN, P. A. E. M. "Quasi-linear theory of wind-wave generation applied to wave forecasting", *Journal of Physical Oceanography*, v. 21, pp. 1631–1642, 1991.

[16] ECMWF. *IFS Documentation CY38r1, Part IV: Physical Processes*, 2013.

[17] RENFREW, I. A., MOORE, G. W. K., GUEST, P. S., et al. "A Comparison of Surface Layer and Surface Turbulent Flux Observations over the Labrador Sea with ECMWF Analyses and NCEP Reanalyses", *Journal of Physical Oceanography*, v. 32, pp. 383–400, 2002.

[18] EDSON, J. B., JAMPANA, V., WELLER, R. A., et al. "On the Exchange of Momentum over the Open Ocean", *Journal of Physical Oceanography*, v. 43, pp. 1589–1610, 2013. Disponível em: <http://dx.doi.org/10.1175/JPO-D-12-0173.1>.

[19] GABIOUX, M. *Estudo Numerico dos Meandros e Vortices da Corrente do Brasil entre 22S E 30S*. Tese de Doutorado, UFRJ, 2008.

[20] ANTONOV, J. I., SEIDOV, D., BOYER, T. P., et al. *World Ocean Atlas 2009, Volume 2: Salinity*. Relatório técnico, Washington, D.C., USA, 2010. Disponível em: <http://www.nodc.noaa.gov/OC5/indprod.html>.

[21] LOCARNINI, R. A., MISHONOV, A. V., ANTONOV, J. I., et al. *World Ocean Atlas 2009, Volume 1: Temperature*. Relatório técnico, Washington, D.C., USA, 2010. Disponível em: <http://www.nodc.noaa.gov/OC5/indprod.html>.

[22] PAIVA, A. M., CHASSIGNET, E. P., MARIANO, A. J. "Numerical simulations of the North Atlantic subtropical gyre: sensitivity to boundary conditions", *Dynamics of Atmospheres and Oceans*, v. 32, pp. 209–237, 2000.

[23] GABIOUX, M., DA COSTA, V. S., DE SOUZA, J. M. A. C., et al. "Modeling The South Atlantic Ocean Fom Medium To High-Resoution", *Revista Brasileira de Geofisica*, v. 31(2), pp. 229–242, 2013.

[24] PAIVA, A. M., CHASSIGNET, E. P. "The Impact of Surface Flux Parameterizations on the Modeling of the North Atlantic Ocean", *Journal of Physical Oceanography*, v. 31, pp. 1860–1879, 2001.

[25] DA SILVEIRA, I. C. A., SCHMIDT, A. C. K., CAMPOS, E. J. D., et al. "A Corrente do Brasil ao Largo da Costa Leste Brasileira", *Brazilian Journal of Oceanography*, v. 48, n. 2, pp. 71–183, 2000. Disponível em: <`http://dx.doi.org.sci-hub.cc/10.1590/S1413-77392000000200008`>.

[26] JULLION, L., HEYWOOD, K. J., GARABATO, A. C. N., et al. "Circulation and Water Mass Modification in the Brazil–Malvinas Confluence", *Journal of Physical Oceanography*, v. 40, pp. 845–864, 2010. doi: 10.1175/2009JPO4174.1.

[27] LARGE, W. G., MCWILLIAMS, J. C., DONEY, S. C. "Oceanic vertical mixing: a review and a model with a nonlocal boundary layer parameterization", *Reviews of Geophysics*, v. 32, pp. 363–403, 1994.

[28] ARDHUIN, F., CHAPRON, B., COLLARD, F. "Observation of swell dissipation across oceans", *Geophysical Research Letters*, v. 36, n. L06607, 2009. doi: 10.1029/2008GL037030.

[29] FAIRALL, C. W., BRADLEY, E. F., HARE, J. E., et al. "Bulk Parameterization of Air–Sea Fluxes: Updates and Verification for the COARE Algorithm", *American Meteorological Society*, v. 16, pp. 571–591, 2003.

[30] HWANG, P. A. "Comparison of Ocean Surface Wind Stress Computed with Different Parameterization Functions of the Drag Coefficient", *Journal of Oceanography*, v. 61, pp. 91–107, 2005.

[31] LIU, B., GUAN, C., XIE, L. "The wave state and sea spray related parameterization of wind stress applicable from low to extreme winds", *Journal of Geophysical Research*, v. 117, 2012. doi: 10.1029/2011JC007786.

[32] OBERMANN, A., EDELMANN, B., AHRENS, B. "Influence of sea surface roughness length parameterization on Mistral and Tramontane simulations", *Advances in Science and Research*, v. 13, 2016.

[33] WU, J. "Wind-stress coefficients over sea surface from breeze to hurricane", *Journal of Geophysical Research*, v. 87, pp. 9704–9706, 1982. doi: 10.1029/JC087iC12p09704.

[34] SAHA, S., OTHERS. "The NCEP Climate Forecast System Reanalysis", *Bulletin of the American Meteorological Society*, pp. 1015–1057, 2010. doi: 10.1175/2010B.

[35] LAWRENCE, M. G. "The Relationship between Relative Humidity and the Dewpoint Temperature in Moist Air - A Simple Conversion and Applications", *Bulletin of the American Meteorological Society*, pp. 225–233, 2005.

# Appendix A

# Additional material

## A.1 Stress statistic results in absolute value (in $N/m^2$)

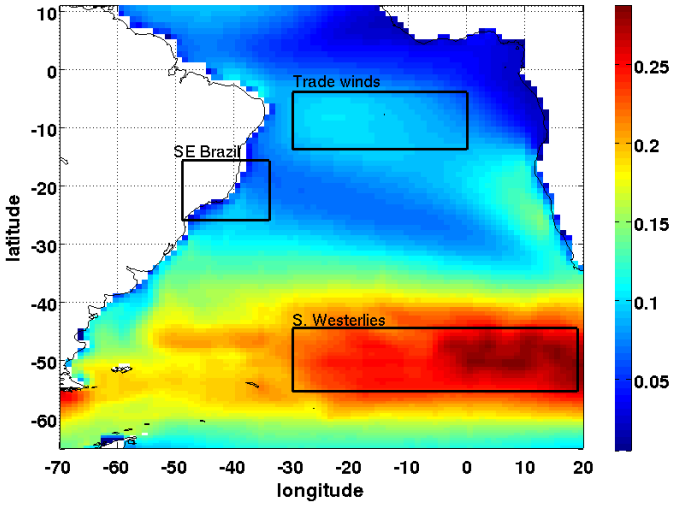


Figure A.1: Mean classic stress, in $N/m^2$ , i.e. $\overline{\tau_{classic}}$ , where the over bar symbol denotes the (time) average for the period 2001-2010. The space-averaged values are $0.15N/m^2$ for the full domain, $0.25N/m^2$ for the Southern Westerly area, $0.09N/m^2$ for the Trade winds area and $0.067N/m^2$ for the SE Brazil area.

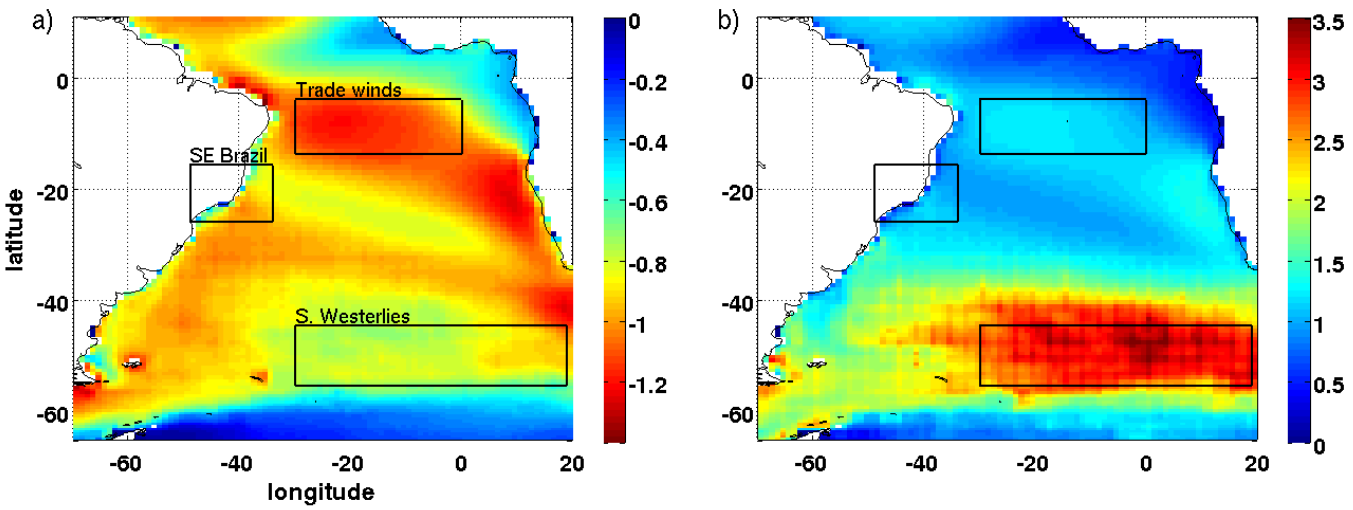


Figure A.2: **Panel a**: Absolute difference of mean classic stresses, in $10^{-2}N/m^2$ , i.e. $(\overline{\tau_{oc}} - \overline{\tau_{classic}}) * 10^2$ , where the over bar symbol denotes the (time) average for the period 2001-2010. The space-averaged values are -0.008$N/m^2$ for the full domain, the Southern Westerly area and the SE Brazil area. The value is -0.011$N/m^2$ for the Trade winds area. **Panel b**: Root Mean Square stress difference, in $10^{-2}N/m^2$, i.e. $\sqrt{1/N * \sum(\tau_{oc} - \tau_{classic})^2} * 10^2$, with $N$ the number of observations for the same period. The space-averaged values are $0.017N/m^2$ for the full domain, $0.03N/m^2$ for the Southern Westerly area, $0.012N/m^2$ for the Trade winds area and $0.009N/m^2$ for the SE Brazil area.

## A.2 Wave effects comparison for the three sub areas

The figure A.3 present for each sub area the comparison between each effect.

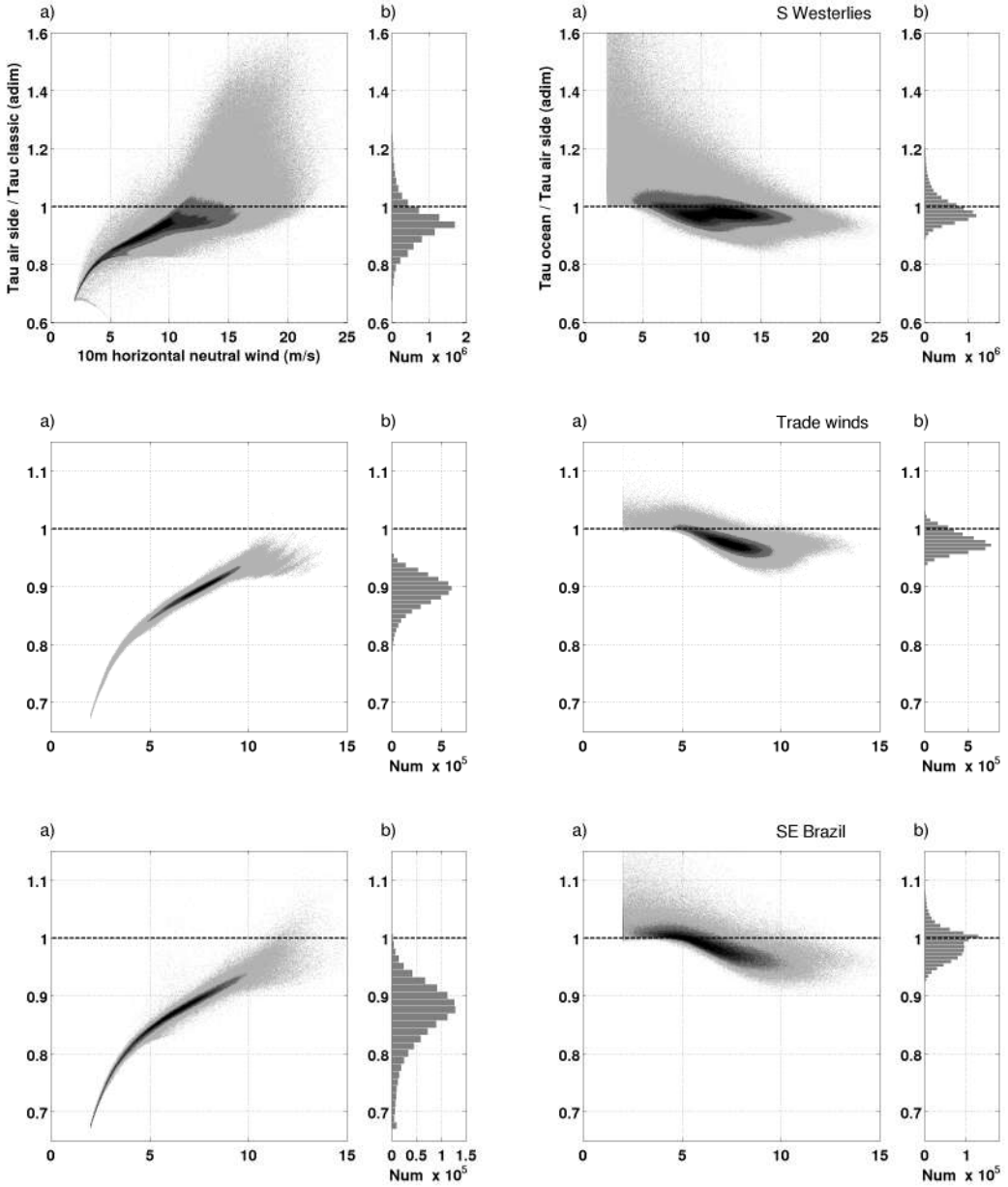


Figure A.3: Stress ratio for the **two wave effects**: Left panel is $\tau_a/\tau_{classic}$ and right panel is $\tau_{ocean}/\tau_a$ for the 2001-2010 period and for **each sub area** from top to bottom: Southern Westerlies, Trade winds, Southeast Brazil. **Panel a**: Scatter data of the ratio plotted against the 10m neutral wind, where each tone of grey represents 25% of the total amount of information (space x time) and a darker grey is a more frequent ratio (4 tones used). **Panel b**: Stress ratio distribution (in number of occurrences for the area) for ranges of ratio.

# Appendix B

# Wave-modified drag coefficient parametrization

$C_D$ parametrization is still the subject of many researches, see for instance FAIRALL *et al.* [29] for the study of the COARE algorithm related to air-sea fluxes, HWANG [30] about reference height of parametrization functions, and more recently wave-influenced parametrizations found in LIU *et al.* [31] or its effects on mesoscale meteorological phenomenon in OBERMANN *et al.* [32]. It could have been in itself a self sufficient thesis subject.

We discuss here the wave-modified drag coefficient we have used and compare it to the classic formulation selected for our study. We describe the reason leading to the selection of the classic formulation. We do not aim at finding which parametrization best fit the reality since we do not have data to compare to and since the objective is more a qualitative comparison (of wave effects) rather than a quantitative one (general behaviour rather than exact figures).

Our approach is practical: we need a wave-modified stress to be compared to a classic, wave-free formulation. The wave-modified formulation has been selected following BREIVIK *et al.* [10] and using available data of ERA-20C (see POLI *et al.* [12]). The classic approach is then selected from the same source to be able to compare our results to the work above mentioned.

## B.1 ECMWF Integrated Forecast System

We give a short description of the ECMWF Integrated Forecast System. It is composed of three coupled models: land, wave and atmosphere models. The main coupling mechanism between the wave and atmosphere models is the wave-modified Charnock coefficient, as presented in equation 2.6 of the section 2.4. The schematic representation of this coupling is shown in figure B.1.

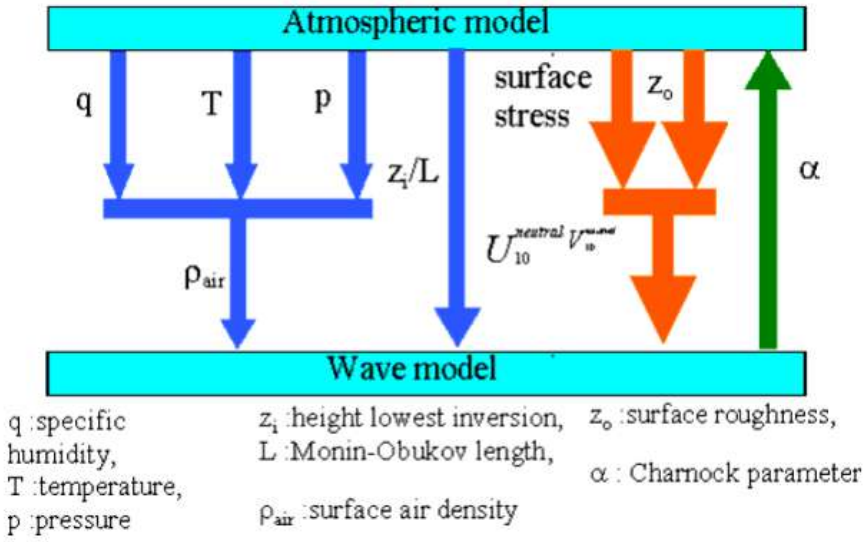


Figure B.1: Schematic representation of the coupling between the atmosphere and wave models of ECMWF, taken from ECMWF [6] figure 3.3

We will now focus on the coupling scheme, describing the following steps:

- computation of stress and roughness length $z_0$ within the atmospheric model
- diagnose of 10-m wind and drag coefficient in the wave model
- production of the wave modified Charnock coefficient by the wave model
- back to the atmospheric model stress and roughness length computation...

The surface stress, going down in the figure B.1 (in orange) is computed within the atmospheric model taking into account the stability: see equations 3.13 and 3.14 from ECMWF [16] for the momentum flux and the momentum transfer coefficients, respectively. The wave and the smooth flow effects are taken into account through a modified Charnock equation for the the roughness length $z_0$. It differs from the original Charnock equation defined in section 2.3 (equation 2.4) in that is has a smooth flow term added to its parametrization and a variable wave-dependent Charnock coefficient $\alpha_{CH}$ (instead of constant one). Following ECMWF [16] equation 3.26, we read for the modified Charnock equation:

$$z_0 = \alpha_M \frac{\nu}{u_*} + \alpha_{CH} \frac{u_*^2}{g} \tag{B.1}$$

where $\nu$ is the air dynamic viscosity and $\alpha_M$ is a smooth flow coefficient. Values of $\alpha_M$ and $\alpha_{CH}$ for various parametrizations can be found in table B.1. The wave-modified Charnock coefficient is provided by the last time step from the wave model.

The neutral wind $U_{10}^n$ used by the wave model is diagnosed at $z = 10m$ based on the above atmospheric (model) stress and roughness length $z_0$, together with the neutral wave-modified drag coefficient $C_{D\,wave}$ within the wave model as follow ($x$-component of vector $\mathbf{U^n}$ shown):

$$U_z^n = \frac{1}{\kappa} \frac{\frac{\tau_x}{\sqrt{\rho_{air}}}}{\left[\tau_x^2 + \tau_y^2\right]^{\frac{1}{4}}} \ln(\frac{z}{z_0}) \tag{B.2}$$

$$C_{D\,wave} = \frac{u_*^2}{||\mathbf{U^n}||^2} \tag{B.3}$$

Note that this is done at a different time step than the atmospheric stress computation and on a different grid, the wave model one. For those reasons (and some differences in the wave assimilation scheme), this wave model neutral wind is a bit different from the wind of the atmospheric model (this one diagnosed within the atmospheric model). The wind and wave-modified drag coefficient downloaded and used in our study are the one from the wave model from equations B.2 and B.3. This wind is the one forcing the wave model WAM (ECMWF [6]).

The wave model is ran with the air-side stress $\tau_a$ and produces all the stresses ($\tau_w$, $\tau_{ds}$ and $\tau_{oc}$) described in sections 2.1 and 2.4. The normalized stress into ocean coefficient $\widetilde{\tau}$ of equation 3.3 is produced and stored at that time. An up-dated wave-modified Charnock coefficient is produced based on equation 2.6 and given to the atmospheric model (upward green arrow of figure B.1). A new coupling cycle then starts again.

## B.2 Neutral Wind

The neutral wind is an equivalent wind (to the 10m horizontal wind) including the effect of the atmospheric boundary layer stability, as can be seen in equation 3.95 of ECMWF [16] for the atmospheric model. It is strongly linked to the neutral drag coefficient and basically comes from the momentum flux equality:

$$C_D^n \, {U_{10}^n}^2 = C_D \, {U_{10}}^2 \tag{B.4}$$

where $C_D^n$ is the drag coefficient in neutral conditions and $C_D$ is the one valid for any stability condition (i.e. it includes the corrections from universal gradient functions of a stability parameter, from the Monin-Obukhov similarity theory). The wave model wind is also neutral since it is derived from the neutral wind profile $\ln(\frac{z}{z_0})$, see equation B.2. The figure B.2 shows the wind distribution for each area as given by the wave model WAM for ERA-20C. One can see that the minimum wind from ERA-20C data is 2 m/s, with some areas (Southeast Brazil and in a lesser way

Southern Westerlies) having probably the lowest bin over represented (the "true distribution" most probably follows the curve shape). This cut-off is assumed to be originated in the various interpolations done during the computation process (different grids due to the coupled numerical models) and the downloading process done on an additional different grid.

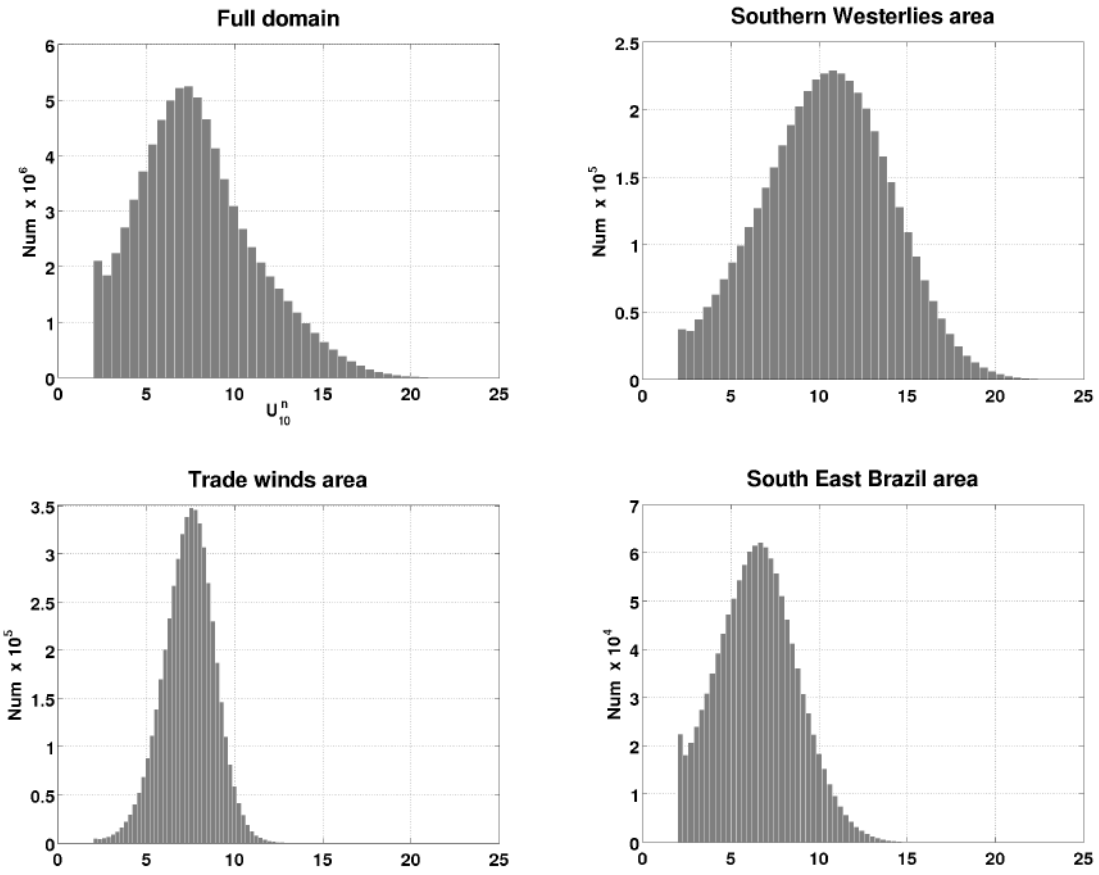


Figure B.2: 10-m neutral wind $U_{10}^n$ (in m/s) distribution from the wave model for each area. Vertical scale varies from one to two orders of magnitudes due to the size of the considered area.

## B.3 Wave-influenced $\alpha_{CH}$ variability: the ratio $\tau_w/\tau_a$

As can be seen in equation 2.6, what drives the variability of the wave-modified Charnock parameter is the ratio $\tau_w/\tau_a$ which represents the ratio of energy retained by the wave field. This explicit part of the parametrization is combined to a 0.006 constant tuned so as to obtain values of the Charnock parameter of 0.0185 for old

wind sea waves in agreement with observations (see WU [33] cited in ECMWF [6] page 15).

We present in figure B.3 the distribution (histogram) of such ratio for the four areas considered. To do so, we need to compute first the wave-modified Charnock $\alpha_{CH}$ coefficient (not available for download) which allows then to retrieve $\tau_w$ from $\tau_a$ and equation (2.6). The Charnock coefficient is computed as follow:

$$\alpha_{CH} = \frac{98.07}{\exp(\frac{0.4}{\sqrt{C_{D\,wave}}})C_{D\,wave}U_{10}^{n\,2}} \tag{B.5}$$

And we get then the sought ratio:

$$\frac{\tau_w}{\tau_a} = 1 - \left(\frac{0.006}{\alpha_{CH}}\right)^2 \tag{B.6}$$

We can see in figure B.3 that the minimum quantity absorbed by wave is around 30% of the wind input and that, in the mean, the absorption percentage is close to 70%, emphasizing the importance of the waves as a medium between the atmosphere and the the ocean. This 0.7 ratio for the whole domain gives a mean Charnock coefficient $\alpha_{CH} = 0,011$ when using the equation 2.6, and ranges from 0.007 (ratio 0.3) to 0.027 (ratio 0.95). This seems consistent with the values found in table B.1. The ocean is in the mean smoother than in the classic parametrization ($\alpha_{CH} = 0.018 > 0.011$).

The highest absorbed quantities are found in the Southern Westerlies area together with the greatest variability. This is consistent with the idea that Southern ocean has the roughest seas, in terms of roughness length $z_0$. The trade winds area has smoother surface roughness together with less variability, consistent with its regular wind intensity over time.

## B.4 Drag coefficients

We present here the two neutral drag coefficients used in this work: $C_{D\,classic}$ and $C_{D\,wave}$, plotted for the four areas in figure B.4 together with the one used in the UFRJ Physical Oceanography Lab - LOF/GRUPO and the REMO network, the NCEP/CFSR formulation. The drag coefficients have been computed in a loop process based on the modified Charnock equation B.1. Its coefficients are taken from RENFREW *et al.* [17] and ECMWF [16] and are recalled in table B.1. One can find the MATLAB code in appendix E.1.

We find a good agreement with figure 7 of RENFREW *et al.* [17] between the ECMWF uncoupled (blue) and CFSR (green) curves relative position, despite the different geographical areas considered (South Atlantic versus Labrador sea). The

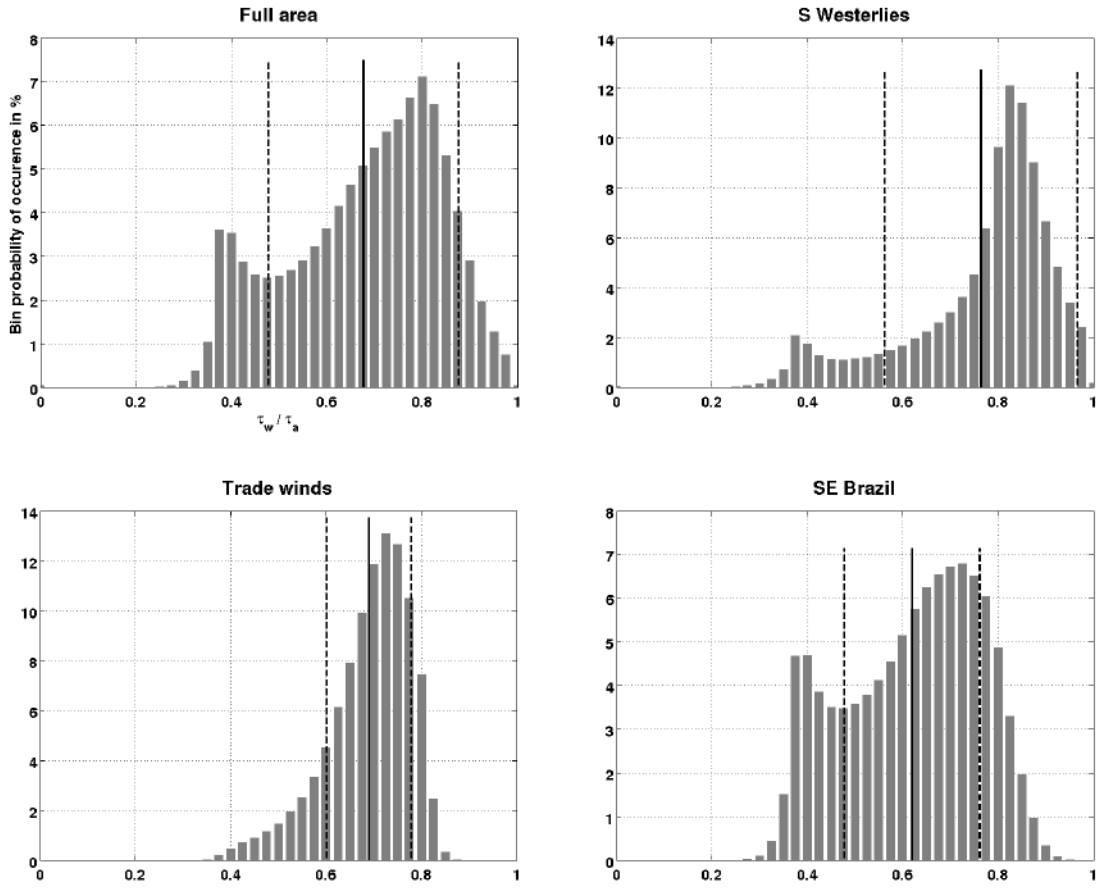


Figure B.3: Wave absorption ratio distribution, i.e. histogram of $\tau_w/\tau_a$ for the various areas considered: Full domain, Southern Westerlies, SE Brazil and Trade winds (clockwise, starting from top left). Each bin contribution is given in % of the total number of observations, the sum of all bins being 100%. The vertical plain line is the mean value and the two doted lines are the mean +/- one standard deviation of the distribution.

| | NCEP | ECMWF (uncoupled) | ECMWF coupled |
|---|---|---|---|
| $\alpha_M$ | 0 | 0.11 | 0.11 |
| $\alpha_{CH}$ | 0.014 | 0.018 | wave-dependant |

Table B.1: Coefficients of the modified Charnock equation B.1 for various parametrizations taken from RENFREW *et al.* [17]. NCEP/CFSR refers to the National Centers for Environmental Prediction (see SAHA *et al.* [34]). ECMWF has two sets of values for uncoupled model, i.e. without wave information (classic approach) and the wave-modified one (coupled models)

CFSR parametrization has a lower drag coefficient for the full wind intensity range in both cases.

Note that the CFSR drag coefficient do not take into account the smooth flow effect ($\alpha_M = 0$). The results seem closer to the mean wave-modified drag coefficient

for the Trade wind area. The definition and use of a drag coefficient is strongly related to the computation scheme and the type of wind used (see HWANG [30]) and this comparison is thus to be considered with great caution. This is partly why the ECMWF formulation has been used for our control experiment, to use a consistent set of variables and coefficients.

The $C_{Dwave}$ considering the full area (upper left panel) has missing values for extreme winds due to the ice zone in the extreme South where it is not defined and where strongest winds occur. The smooth flow effect cannot be seen in the wave-modified drag coefficient (red curve) due to the way it is generated (together with the neutral wind) in the coupled models scheme, see section B.1. The smooth flow effect is somewhat melted in the wind / drag coefficient combination. But it is accounted for, since the smooth flow term of equation B.1 is taken into account in the atmospheric model.

The wave effect bring large variability, especially for winds in excess of 10 m/s in the Southern Westerlies and SE Brazil areas. The Trade winds area has almost no variability brought by the waves and the drag coefficient is always lesser for than the classic ECMWF formulation.

In conclusion of this annex we have found in the wave-modified drag coefficient parametrization the same behaviour that the one explored in section 3.3: a lesser mean value and more variability brought by the wave field. We have linked the explicit part of the parametrization (the wave absorption ratio) to its effects on the roughness of the sea surface and showed a good agreement of the parametrization and the ERA-20C data with the physical characteristics of our areas of interest. The retained parametrizations of the drag coefficients (classic approach and first wave effect) are therefore consistent with each other since their relative variation matches with the physical process played by the wave field (smaller mean and more variability).

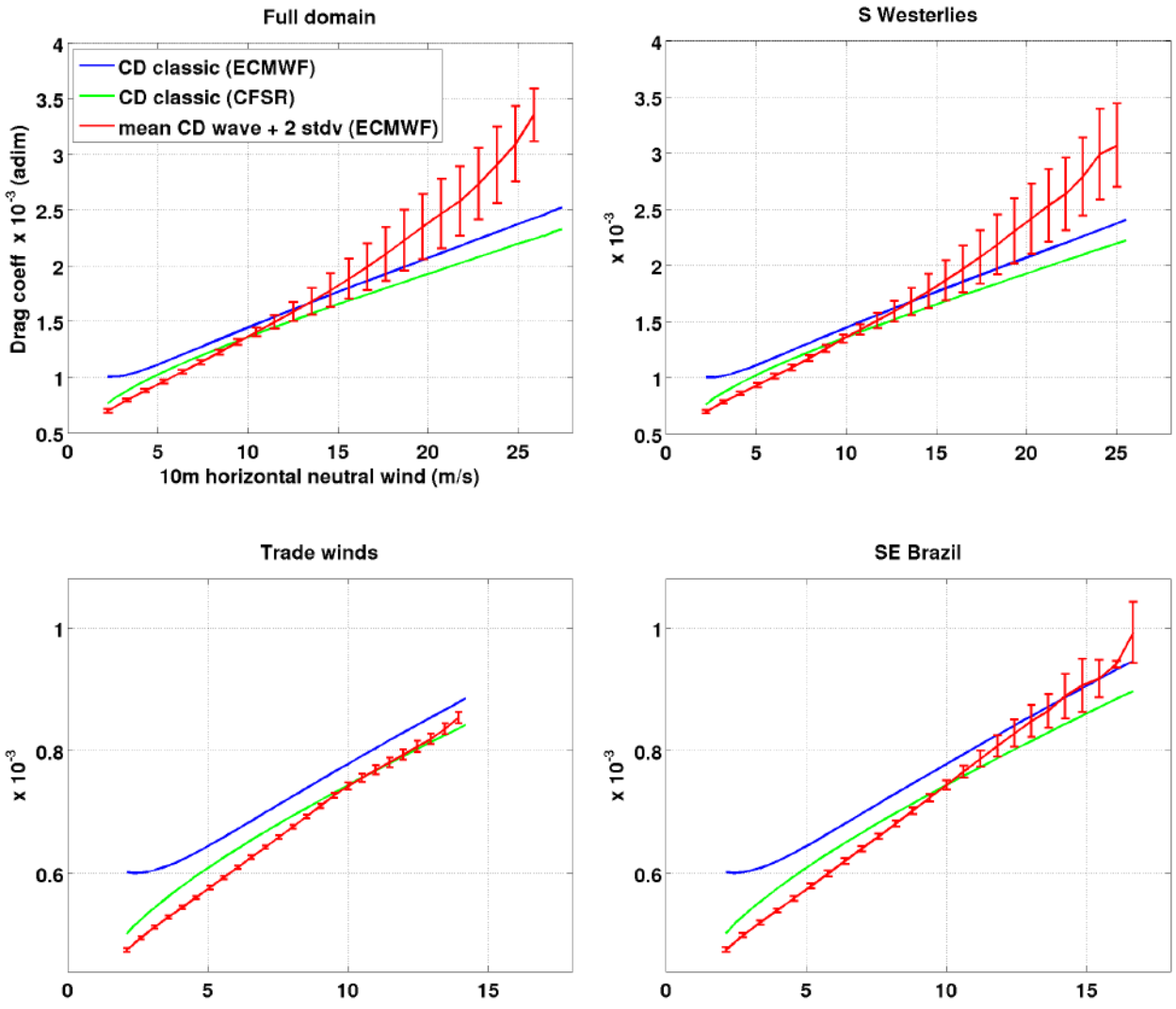


Figure B.4: Drag coefficients for the four areas. The blue curve is the ECMWF formulation (smooth flow effect included). The green one is the NOAA/CFSR formulation (no smooth flow). The red curve is ECMWF wave-modified mean drag coefficient with two standard deviations vertically plotted. Note the difference of scales between the upper and lower panels

# Appendix C

# HYCOM model

We present here some complementary results to the chapter 4, useful for illustration. The first section C.1 gives details on the downloading tool used, the data management and the mixing ratio calculation. Section C.2 shows the bathymetry used (figure C.1) and provides more results of the general behaviour of the two experiments. The time evolution of the region-wide mean values of SSH, T, S and density is shown in figure C.2. The figure C.3 presents the time evolution of the mixed-layer mean parameters. Figures C.4 and C.6 show meridional sections at 25° W for the mean temperature comparison to WOA2009 and the differences in temperature and salinity (brought by the wave effects) respectively. The figure C.5 shows the mean speed in the 2D section defined in section 4.2 and the time variation of the integrated Brazil Current transport (right panel) where the seasonality is well seen. The mean wave effect on mixed layer depth is shown in figure C.7 (right panel) together with the classic approach mean value (CTRL run).

## C.1 HYCOM forcing fields production

ERA-20C reanalysis data is downloaded from the Meteorological Archival and Retrieval System (MARS) of ECMWF. MARS is a web API allowing to download data in a programmatic way based on Python scripts. The data consists of spatial 2D fields at each time step with no gap, i.e. the missing values are filled with the minimum value from each 2D field (e.g. ocean data over land, or wave model results over ice). This has been used to filter out the non-desired values over ice and land and led to some data losing since one point (the smallest real value) is removed at each time step and replaced by a "NaN". We have assumed this information loss negligible.

In addition to the surface stresses described in 3.1, the other sea surface parameters necessary to force HYCOM are: the wind speed, the wind direction (to get the

zonal and meridional components of stresses), the 2-meter temperature, the mixing ratio $r_v$, precipitation, the net solar (short wave) radiation and the net thermal (long wave) radiation. All are directly available from ERA-20C (in instantaneous or accumulated fields) as surface fields except for the mixing ratio which is calculated based on the mean sea level pressure $p$ and the dew point temperature $T_{dp}$ as follow:

$$r_v = 0.622 \, \frac{e}{p - e} \tag{C.1}$$

where $e$ is the vapor pressure calculated following the modified equation (7) of LAWRENCE [35]:

$$e = 6.112 \, \exp\left(\frac{17.67 \, (T_{dp} - 273.15)}{T_{dp} - 273.15 + 243.5}\right) \tag{C.2}$$

## C.2 HYCOM model complementary results

We present here the bathymetry, the evolution of the model-wide integrated kinematic energy and the mixed layer depth results.

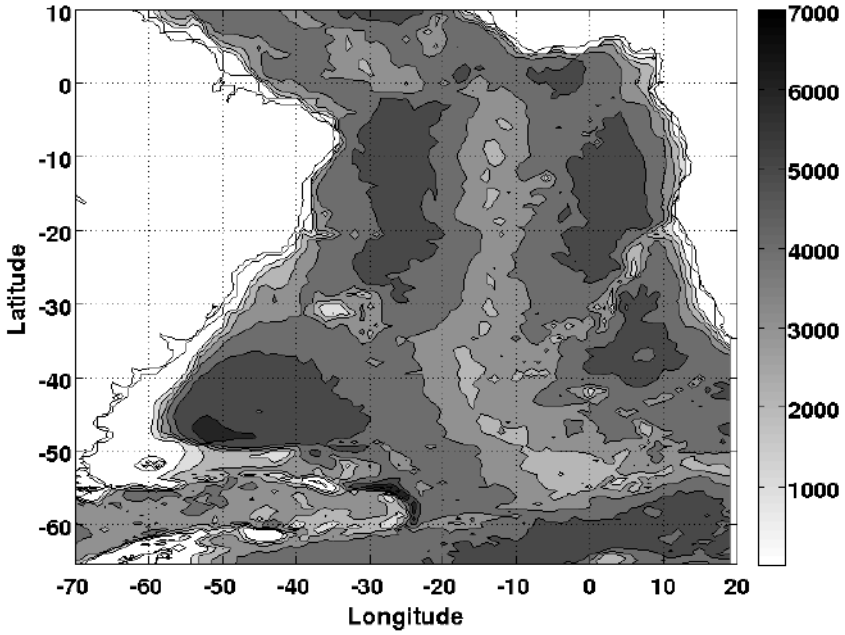


Figure C.1: ETOPO2 bathymetry, in meters.

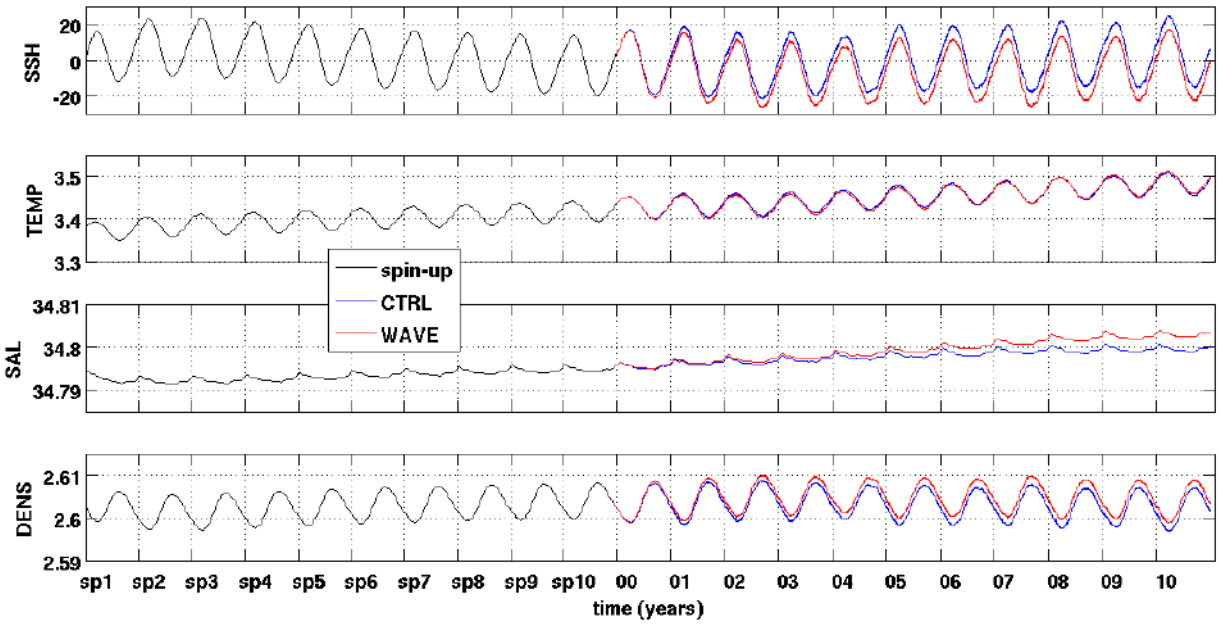


Figure C.2: Region-wide SSH (in meters), Temperature, Salinity and Density anomaly (in $kg/m^3/10$) time series.

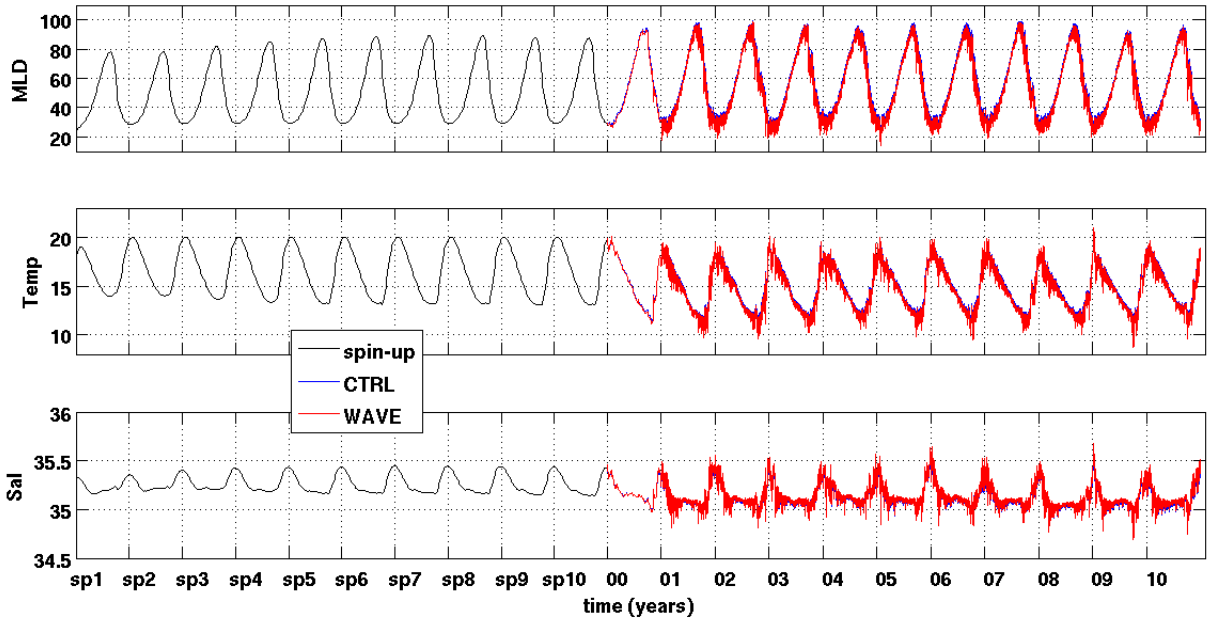


Figure C.3: Region-wide ML time series (depth in meters, temperature and salinity).

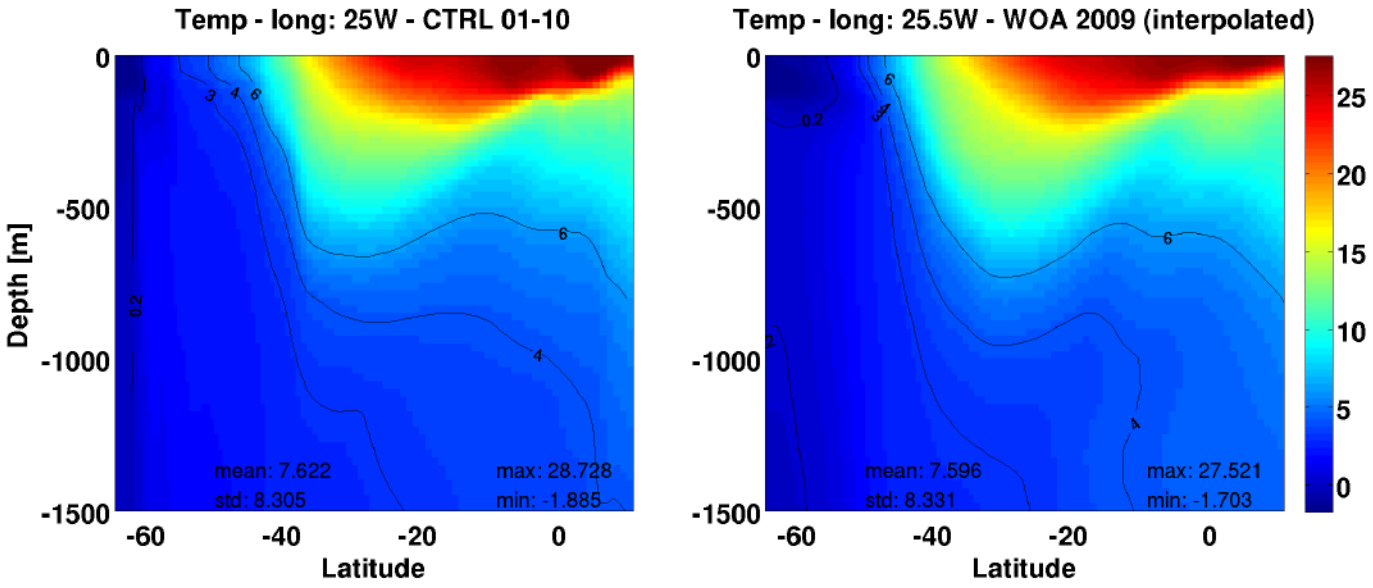


Figure C.4: Meridional section at 25W of mean temperature (in degrees Celsius) between surface and 1500m depth. Left panel: 2001-2010 mean value from HYCOM integration (CTRL run). Right panel: WOA 2009 climatology values interpolated on HYCOM grid results.

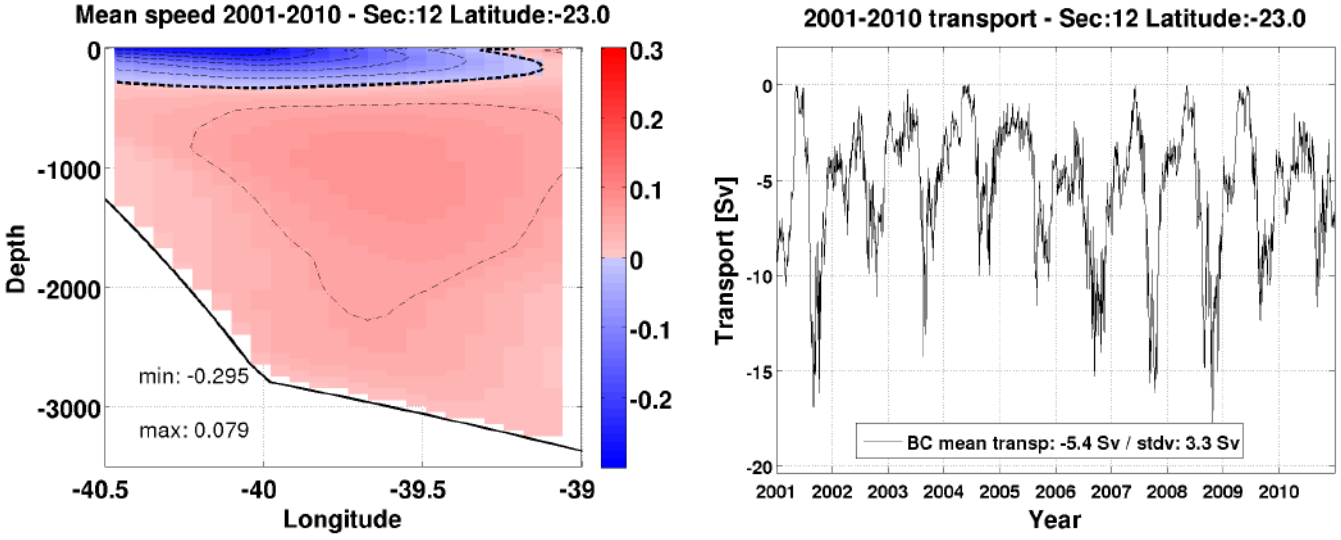


Figure C.5: Brazil Current transport at 23S for the CTRL experiment. **Panel a**: 2D section (lon/lat: from 42W/22S to 39W/24S) showing mean speed perpendicular to the section. **Panel b**: Integrated Southward transport along time.

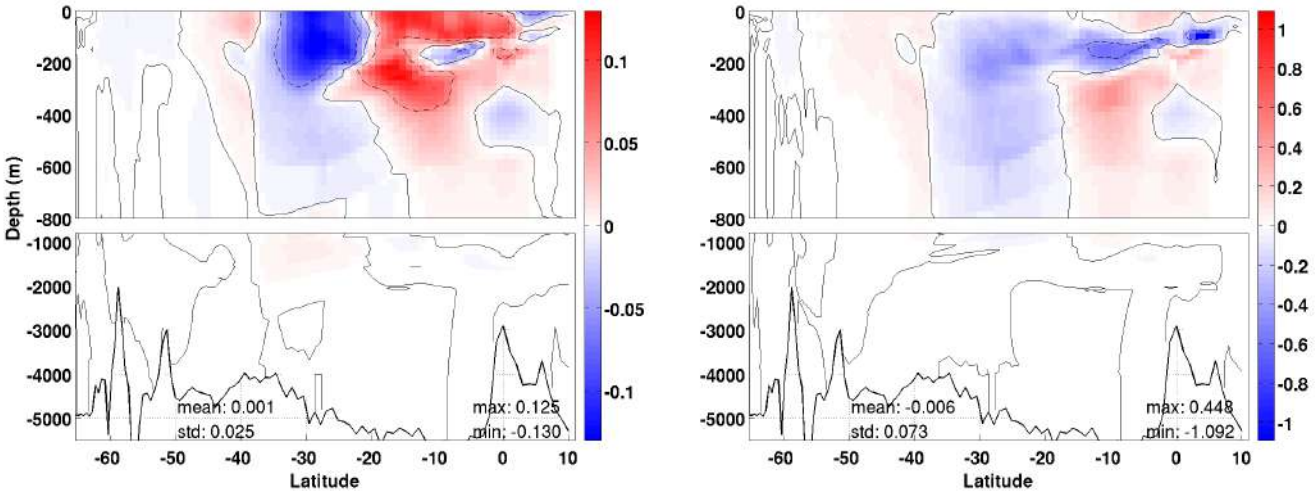


Figure C.6: Meridional section at 25W of mean salinity and temperature differences under wave influence between surface and 5500m depth. **Left panel**: 2001-2010 mean salinity difference ($\overline{S}(\tau_{ocean}) - \overline{S}(\tau_{classic})$). **Right panel**: mean temperature difference. The contour of zero difference is plotted on both panels (continuous line) on top of colour shading. The doted/mixed lines for salinity (temperature) difference are the +0.05/-0.05 (+0.5/-0.5) contours. The mean difference is globally zero, respecting the density equilibrium. The wave effects are mainly restricted to the first 800 meters below the ocean surface.

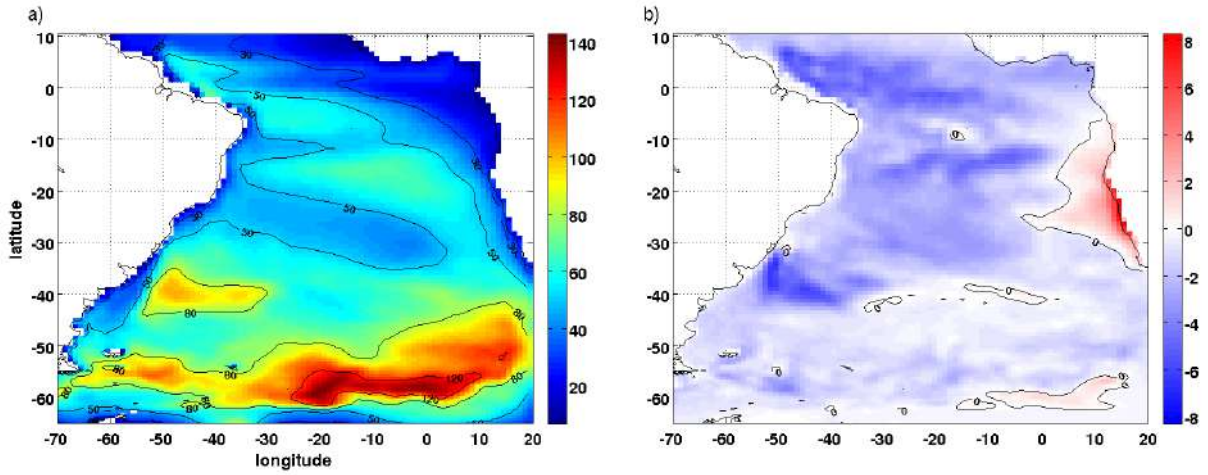


Figure C.7: Mixed Layer Depth long term results. **Panel a**: mean Mixed Layer Depth (in meters) over the period 2001-2010 for the CTRL experiment. The **Panel b** is the long term difference of MLD between the WAVE experiment and the reference (CTRL run), in meters.

# Appendix D

# Discussion

We give in this appendix some additional results to the chapter 5, useful for illustration. The figure D.1 shows the boxplot comparison between the two experiments of SST bias, i.e. $\overline{SST}(\tau_{classic}) - \overline{SST}(WOA2009)$ (blue boxes) and $\overline{SST}(\tau_{ocean}) - \overline{SST}(WOA2009)$ (red boxes). Figures D.2 to D.5 show the same results as discussed in chapter 5 but for reduced areas. Figure D.6 presents some comparison of the SSH with climatology satellite data. Finally, the figure D.7 shows the scatter plot of surface current difference (without any average, in contrast with the Hovmöller results of section 4.3) against the wind speed and the distribution for the wind range 13-15 m/s.

## D.1 Long-term

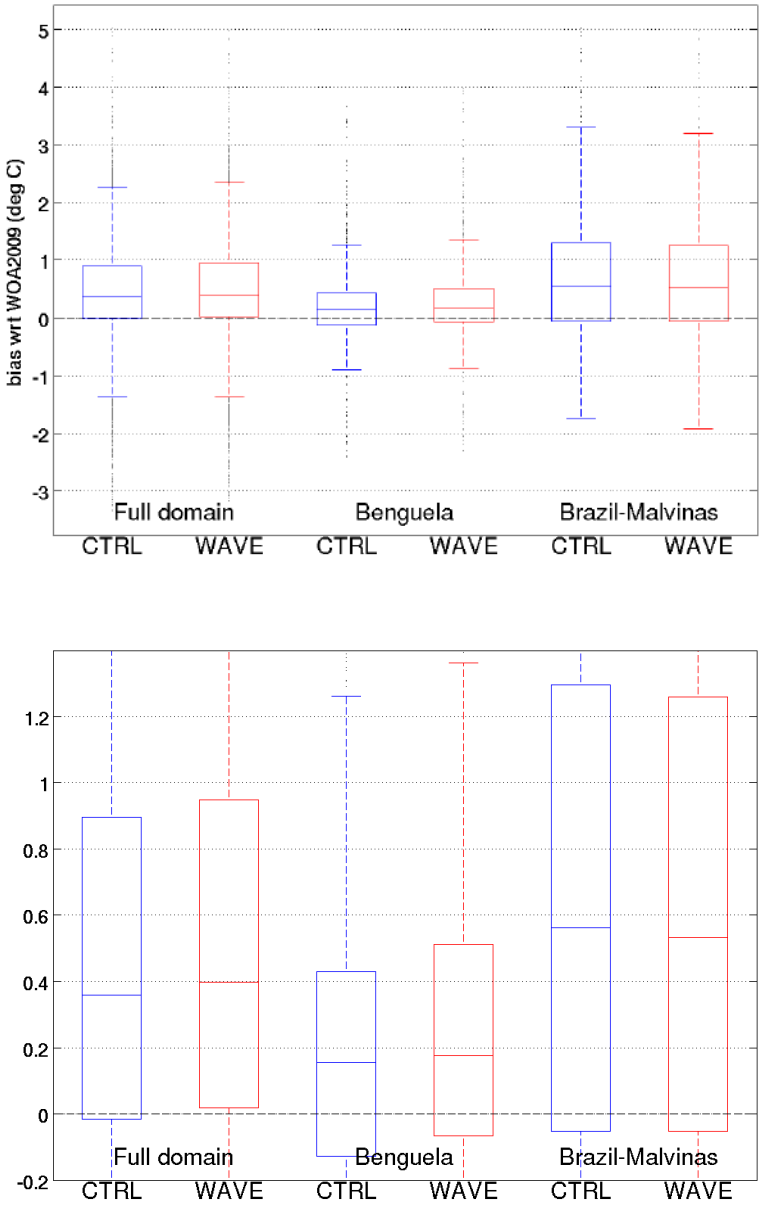


Figure D.1: SST bias comparison in boxplot for three areas (full domain and areas shown in figures D.2 and D.4) under classic forcing (CTRL run, blue) and wave-modified surface stress (WAVE run, red). The lower panel is a zoomed view of the upper one. On each box, the central mark is the median, the edges of the box are the 25th and 75th percentiles, the whiskers extend to the most extreme data points not considered outliers, and outliers are plotted individually (black). Points are drawn as outliers if they are larger than q3 + 1.5(q3 – q1) or smaller than q1 – 1.5(q3 – q1), where q1 and q3 are the 25th and 75th percentiles, respectively.

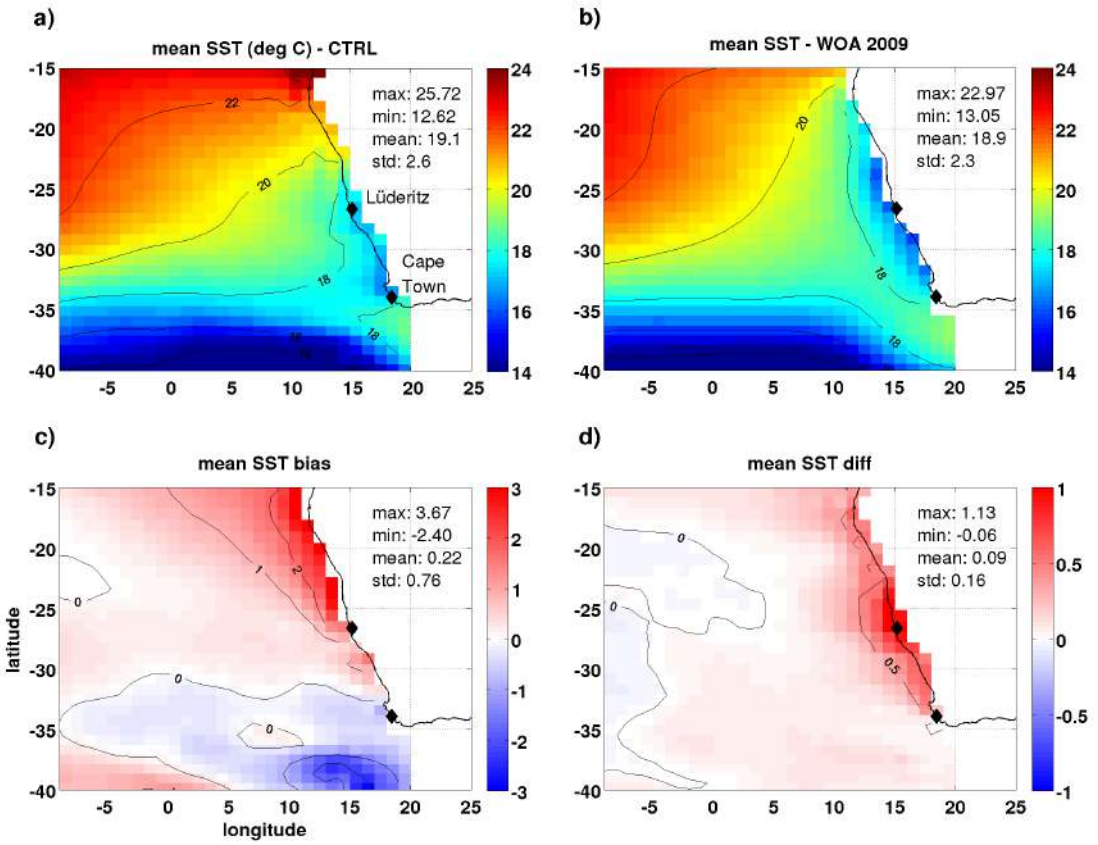


Figure D.2: Long-term Sea Surface Temperature comparison near the Benguela upwelling area. **Panel a**: SST results for the CTRL run. **Panel b**: WOA2009 climatology results. **Panel c**: SST bias of classic approach (CTRL - WOA09). **Panel d**: SST difference (WAVE - CTRL). Note that the classic approach performs better in this situation (wave-modified upwelling is actually warmer) even if the tendency between the two HYCOM runs (panel d) is consistent with BREIVIK *et al.* [10].

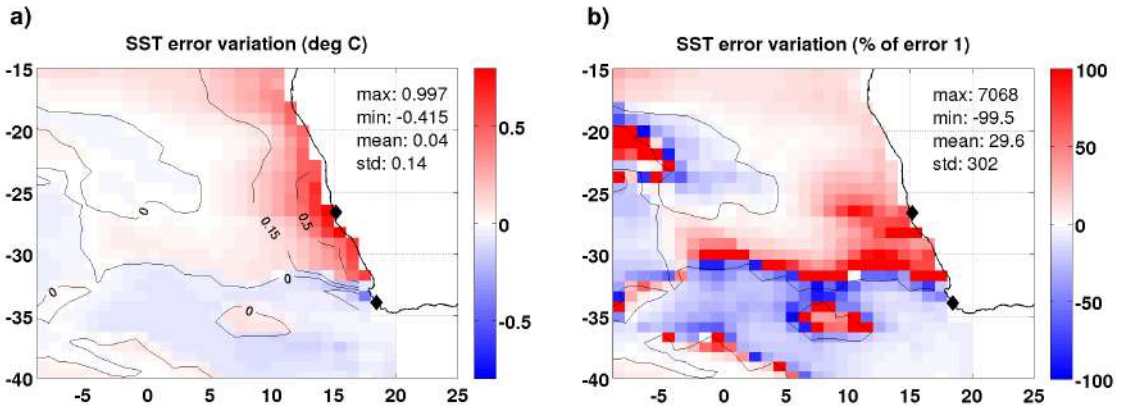


Figure D.3: Benguela upwelling area Sea Surface Temperature error variation. **Panel a**: Absolute error variation, i.e. |WAVE - WOA09| - |CLRL - WOA09|. **Panel b**: Relative error variation, i.e. |WAVE - WOA09| - |CLRL - WOA09| / |CLRL - WOA09|.

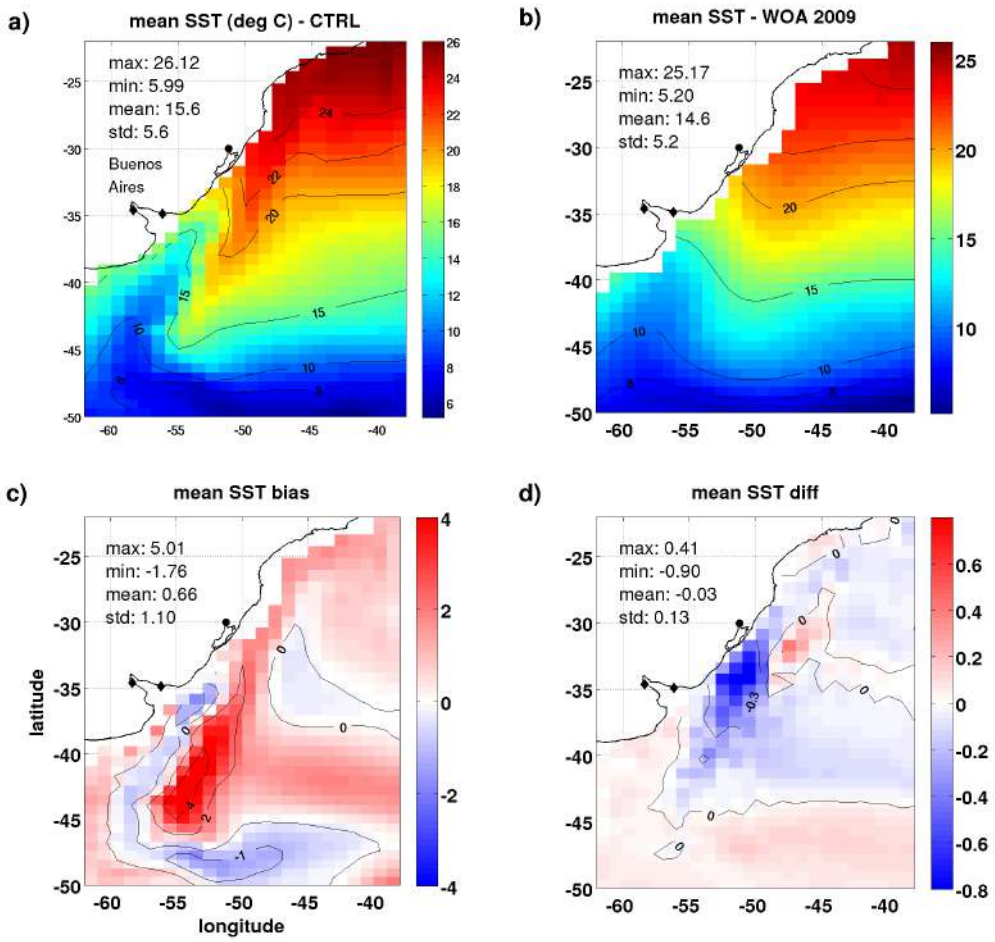


Figure D.4: Long-term Sea Surface Temperature comparison near the Brazil-Malvinas confluence. **Panel a**: SST results for the CTRL run. **Panel b**: WOA2009 climatology results. **Panel c**: SST bias of classic approach (CTRL - WOA09). **Panel d**: SST difference (WAVE - CTRL).

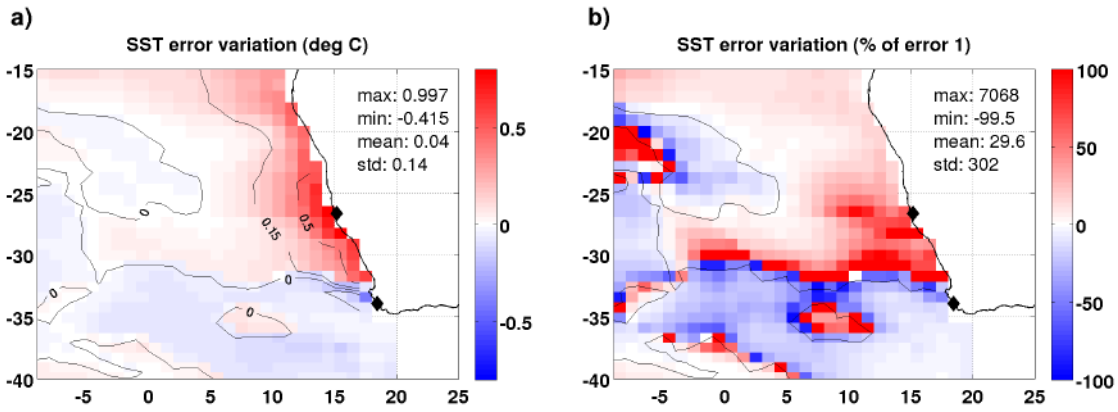


Figure D.5: Sea Surface Temperature error variation near the Brazil-Malvinas confluence area. **Panel a**: Absolute error variation, i.e. |WAVE - WOA09| - |CLRL - WOA09|. **Panel b**: Relative error variation, i.e. |WAVE - WOA09| - |CLRL - WOA09| / |CLRL - WOA09|.

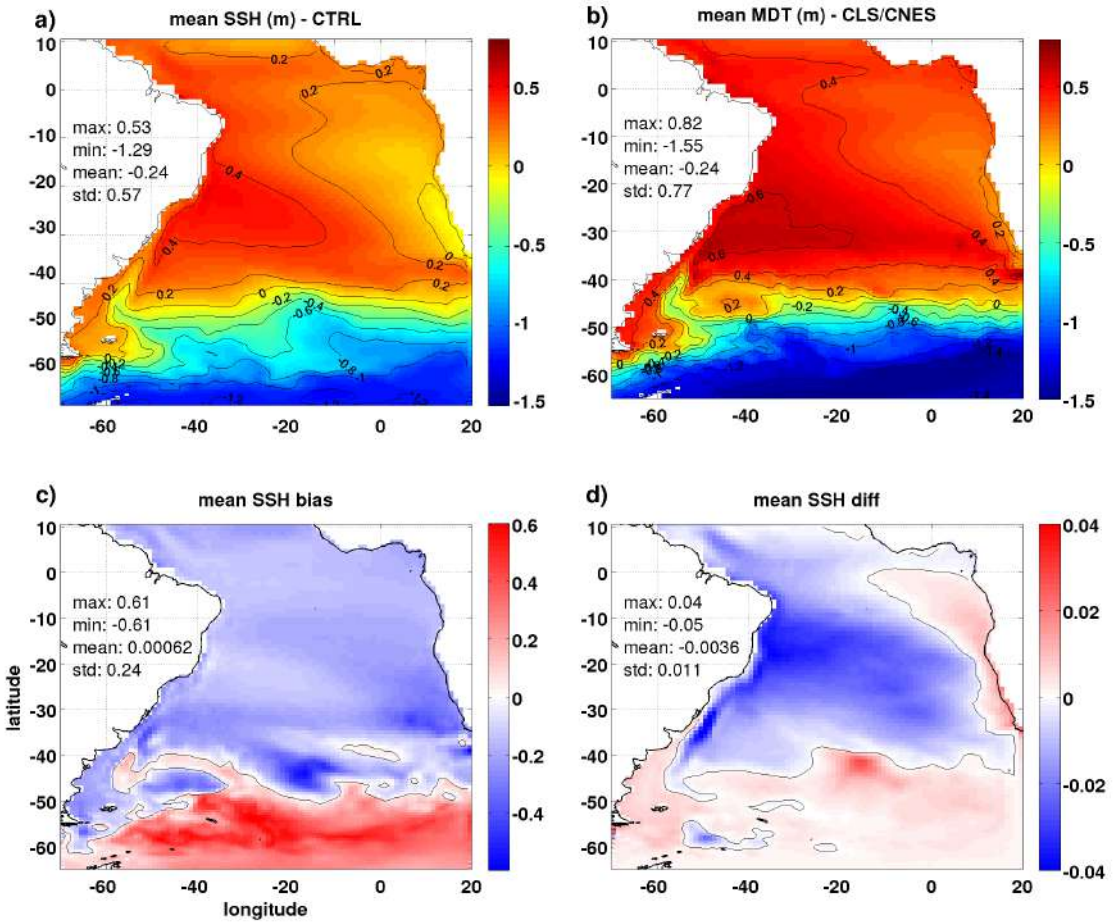


Figure D.6: Long-term Sea Surface Height comparison. **Panel a**: SSH results for the CTRL run. **Panel b**: AVISO/CLS climatology results. **Panel c**: SSH bias of classic approach (CTRL - CLS). **Panel d**: SSH difference (WAVE - CTRL).

## D.2 Single events

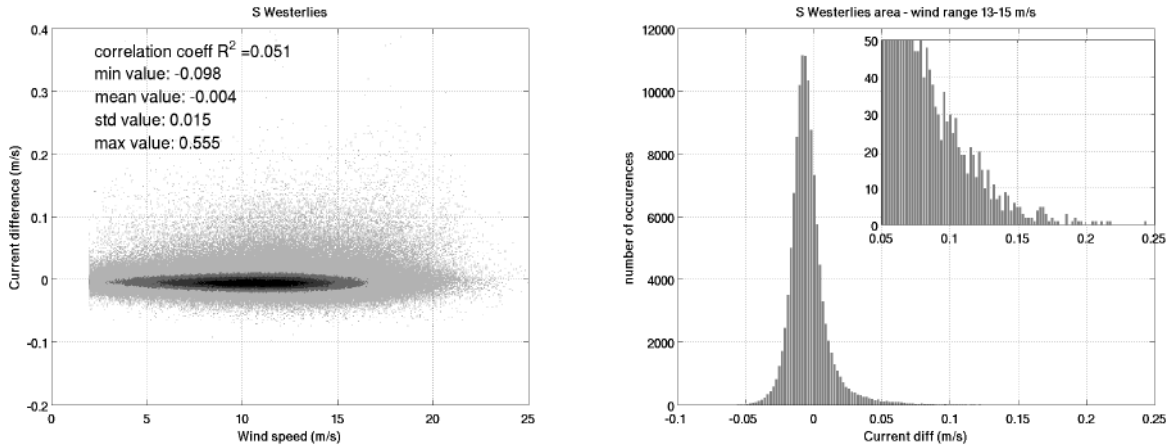


Figure D.7: Surface current difference (i.e. $U_{surf}(\tau_{ocean}) - U_{surf}(\tau_{classic})$) versus wind speed for the year 2006 in the Southern Westerlies area. **Left panel**: Scatter plot of surface current difference versus wind speed. **Right panel**: Distribution of current difference (in number of occurrences) for the 13-15 m/s range (inserted is a zoom of the tail of the distribution).

# Appendix E

# Selected code examples

## E.1 Drag coefficient loop

Here below is the MATLAB code used to compute the classic drag coefficient (see sections 2.3, 3.1 and appendix B). The variables are 3-dimension variables for the physical parameters that vary in 2D space (sea surface) and time. The drag coefficient precision of the "worst" point is achieved within 4 to 6 loops in few seconds thanks to MATLAB efficient matrix libraries (taken from `C` language) even for a 10 years period (RAM memory is the limitation).

```
%%%%%%%%%%%%%%%%%%%%%%%%%%%%%%%%%%%%%%%%%%%%%%%%%%%%%%%%%%%%%%%%%%%%%%%
%%%%%%% HYCOM USED ONE - CD CLASSIC NO WAVE EFFECT
%%%%%%%%%%%%%%%%%%%%%%%%%%%%%%%%%%%%%%%%%%%%%%%%%%%%%%%%%%%%%%%%%%%%%%%
%%% LOOP to calculate CD based on u* and
%%% roughness length z0 (neutral wind U10N used here)

g = 9.807;
%%% air dynamic viscosity (m2/s) from ECMWF IFS Cy38r1 Part 4 chap 3.2.4
nu = 1.5 *10^-5;

%%% Renfrew et al (2002) table A.1 for ECMWF or NCEP coeff
%%% ECMWF
alpha_charn = 0.018;
sm_fl = 0.11;

%%% First guess - formula (32) of Breivik et al (2015)
CD_0 = ( 1.03 *10^-3 + 0.04 *10^-3 .* wind.^1.48 ) ./ wind.^0.21;

%%% Max error for loop
limit_error_CD = 0.0001 * min(min(min(CD_0)));

loop = 0;
CD_temp = CD_0;
```

```
u_star2 = CD_temp .* wind.^2;

z0 = alpha_charn .* u_star2 ./ g + sm_fl * nu ./ u_star2.^0.5;
CD = 0.16 / log(10/z0).^2;

while abs(min(min(min(CD - CD_temp))) ) > limit_error_CD && loop<50
  loop = loop+1;
  CD=CD_temp;
  u_star2 = CD .* wind.^2;
  z0 = alpha_charn .* u_star2 ./ g + sm_fl * nu ./ u_star2.^0.5;
  CD_temp = 0.16 / log(10/z0).^2;
end

disp(['number of iterations to reach desired accuracy ...
  (',num2str(limit_error_CD/min(min(min(CD_0)))), ...
  ' * min(cd ini)) on cd is: ',num2str(loop)])

CD=CD_temp;
```

## E.2 Wave age computation loop

The wave age is computed from the mean wave period (based on spectral $1^{st}$ moment) and 10-m neutral wind speed both downloaded from ERA-20C data base. The phase velocity $c_p$ is first computed based on the wave period ans the dispersion relation. All physical parameters are 3-dimensional.

```
%%%%%%%%%%%%%%%%%%%%%%%%%%%%%%%%%%%%%%%%%%%%%%%%
%%%%%%% WAVE PHASE SPEED AND WAVE AGES
%%%%%%%%%%%%%%%%%%%%%%%%%%%%%%%%%%%%%%%%%%%%%%%%

w=2*pi./mp1;    %%%%% mp1 Mean wave period based on first moment

precision=0.001;                %%% for dispersion relation loop
loop=0;
k_deep = w.^2/9.807;         %%% deep water case
kh01=k_deep.*HHH;          %%% HHH is ''3D'' bathymetry matrix
                           %%% (2D repeated over time)
kh00=0;

if nanmin(nanmin(nanmin(kh01))) > 5         %%% deep water criteria
  k_w = kh01 ./ HHH;
else
    while nanmax(nanmax(nanmax(abs(kh00 - kh01) ./ kh01))) > precision
        loop=loop+1;
        if kh00 == 0
```

```
                kh00 = kh01;
            end
            kh00 = (kh00 + kh01) / 2;
            kh01 = k_deep  .* HHH ./ tanh(kh00);
        end
        k_w = kh01 ./ HHH;
    end
    disp(['wave phase speed - nb of iterations is: ',num2str(loop)])
    clear kh00 kh01 loop
    c_phase_w = w ./ k_w;
    clear w k_w
    w_age_w = c_phase_w ./ wind;
    clear c_phase_w
```